Journal of the Mechanics and Physics of Solids 61 (2013) 1464–1488

Contents lists available at SciVerse ScienceDirect

Journal of the Mechanics and Physics of Solids

journal homepage: www.elsevier.com/locate/jmps

Propagation of Slepyan's crack in a non-uniform elastic lattice

M.J. Nieves [a,*], A.B. Movchan [b], I.S. Jones [a], G.S. Mishuris [c]

[a] School of Engineering, John Moores University, James Parsons Building, Byrom Street, Liverpool L3 3AF, UK
[b] Department of Mathematical Sciences, University of Liverpool, Liverpool L69 3BX, UK
[c] Institute of Mathematics and Physics, Aberystwyth University, Aberystwyth SY23 3BZ, UK

ARTICLE INFO

Article history:
Received 16 February 2012
Received in revised form
26 November 2012
Accepted 28 December 2012
Available online 8 January 2013

Keywords:
Inhomogeneous lattice
Semi-infinite crack
Wiener–Hopf technique
Energy release rate ratio
Stress intensity factor

ABSTRACT

We model and derive the solution for the problem of a Mode I semi-infinite crack propagating in a discrete triangular lattice with bonds having a contrast in stiffness in the principal lattice directions. The corresponding Green's kernel is found and from this wave dispersion dependencies are obtained in explicit form. An equation of the Wiener–Hopf type is also derived and solved along the crack face, in order to compute the stress intensity factor for the semi-infinite crack. The crack stability is analysed via the evaluation of the energy release rate for different contrasts in stiffness of the bonds.

1. Introduction

Models for cracks propagating in lattices have been extensively studied in Slepyan (2002) and Marder and Gross (1995). As noted in Marder and Gross (1995), discrete models enable one to answer fundamental questions about the influence of the micro-structure on the crack motion, and in particular, about the origins of crack instability. Marder and Gross have observed that analytical models of cracks in a lattice involve bond-breaking terms, which are in general non-linear. They have also noted that a nonlinear interaction can be approximated by a linear interaction if bonds along the crack break in sequence. A fracture criterion is also an important part of a numerical simulation describing advance of a crack through a lattice.

We make an emphasis on non-uniformity within a lattice, which can bring new effects in the wave dispersion and filtering properties of the structure. These non-uniformities may be caused, for example, by thermal pre-stress of a constrained lattice whose ligaments have different coefficients of thermal expansion. Linearisation near the pre-stressed state may lead to a model of a lattice with contrasting stiffnesses of bonds. An important example corresponds to stratified systems represented by a triangular lattice, where the stiffness of horizontal bonds differs from the stiffness of other bonds. Such an elastic lattice, containing a moving crack, is analysed in the present paper. Throughout the text, we use the notion of the moving system of coordinates linked to the crack tip. While the emphasis here is made on the analytical findings, the computational models for different fracture criteria are of paramount importance. A separate computational study of advancing crack, based on a deformational fracture criterion, has been presented in Slepyan and

* Corresponding author. Tel.: +44 151 231 2253.
E-mail address: M.J.Nieves@ljmu.ac.uk (M.J. Nieves).

0022-5096/$ - see front matter © 2013 Elsevier Ltd. All rights reserved.
http://dx.doi.org/10.1016/j.jmps.2012.12.006

Ayzenberg-Stepanenko (2002) for the homogenous triangular lattice, and in Colquitt et al. (2012) for the case when the lattice is not uniform.

The full analytical solution is derived here in terms of Fourier transforms for a general type of load following the moving crack. For practical computations, the load has been chosen as in Slepyan (2002) to represent the remote force distant from the crack tip.

Problems involving inhomogeneous lattices containing semi-infinite cracks have been recently analysed. Examples include those containing particles of contrasting mass (Mishuris et al., 2007), and the dynamic extraction of a chain within the lattice (Mishuris et al., 2008).

The propagation of the crack may be caused by feeding waves, generated by some remote source, which lead to the breaking of subsequent bonds within the lattice. Feeding waves bring energy to the crack-front bonds which cause their disintegration one by one and this produces dissipative waves which carry energy away from the front. This process has been investigated in Slepyan (2001a), where Mode III crack propagation within a square-cell lattice is considered, under the assumption of uniform straight line crack growth, and steady state solutions have been obtained. The lattice is assumed to have bonds of identical stiffness which connect particles having a common mass.

The analysis of Mode I and II crack propagation in a uniform discrete triangular lattice was studied in Slepyan (2001b). Compared to the case of the square-cell lattice, the equations of motion relate components of the vector field of displacements. It has been shown that both the solution to this problem and the explicit form of wave dispersion relations can be obtained.

From these lattice models, it is possible to determine the regions of crack speeds for which we have steady state crack motion, and the stability of these states can also be determined by computing the energy release rate for the crack. This has been examined in Fineberg and Marder (1999), Marder and Gross (1995) and Marder and Liu (1993). Another application for a lattice problem is found in Slepyan et al. (2010). Here, the model describing a structured interface along a crack with a harmonic feeding wave localised at the faces was used to predict the position of the crack front. Numerical simulations were presented in Mishuris et al. (2009a) and Slepyan et al. (2010) showing that, for a given range of frequencies of the feeding wave, it was possible to have uniform crack growth or, in the non-linear regime of non-steady propagation, to identify an average crack speed, which is consistent with the prediction of the linear model linked to the crack propagating steadily.

The method of solution of these problems involves formulating the discrete lattice problem in terms of the Fourier transforms of functions describing the displacements (Mishuris et al., 2009b). A Wiener–Hopf functional equation is then derived along the crack faces and factorised to obtain the solution. The kernel in the Wiener–Hopf equation has the interpretation of the Fourier transform of the derivatives of Green's kernel. Similar features also appear in continuum models of cracks which are solved using singular integral equation techniques.

In this paper, using the method in Slepyan (2001b), our main goal is to solve the problem for a discrete triangular lattice, which is constrained at infinity, containing a semi-infinite crack with additional inhomogeneities being brought by the inclined bonds having a contrast in stiffness to the horizontal bonds (see Fig. 1). This contrast in stiffness may arise as an effect of thermal pre-stress, for instance, heating a lattice with bonds that have different coefficients of thermal expansion in the principal directions. The problem for a crack in the uniform triangular lattice has been studied in Slepyan (2002, Chapter 12).

The plan of the paper is as follows. Section 2 includes the description of the problem for a two dimensional lattice with a semi-infinite crack, containing particles of common mass with bonds having contrasting stiffnesses in the principal directions. In Section 3, we rewrite the problem for the lattice using the continuous Fourier transform in the crack line direction, and these equations are solved for the displacements of a particle inside the lattice. A Wiener–Hopf equation for particles along the line of the crack is then written in Section 4 and the representation of the kernel function of this equation is derived. An analysis of the dispersion relations obtained from the roots and poles of the kernel function is carried out in Section 5. In Section 6, we solve the Wiener–Hopf equation of Section 4. In Section 7, we evaluate the energy

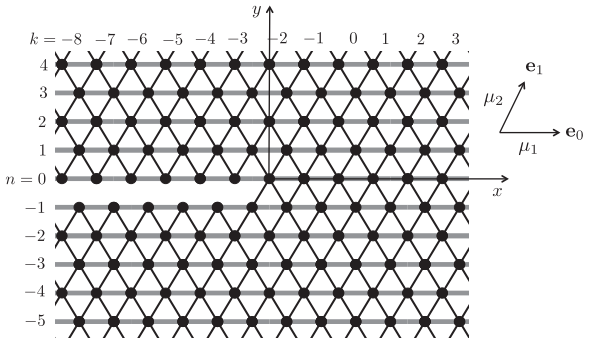

Fig. 1. The inhomogeneous lattice containing a semi-infinite crack showing the lattice coordinates. The crack is located between the rows $n=-1$ and $n=0$.

release rate for the crack propagating through the inhomogeneous lattice and investigate its sensitivity to the crack speed and to the stiffness contrast. We compute the stress intensity factor for the semi-infinite crack propagating through the inhomogeneous lattice and show its behaviour, for different stiffness contrasts, as a function of the crack speed in Section 8. In Section 9, we give conclusions on the results presented here.

In addition to the main text of the paper, we also provide Appendices which include more details of the derivations of the results contained in the main body of the paper. In Appendix A, the coefficient of the leading order term of the asymptotics for the kernel function near the zero wavenumber is studied. Some comments relating to the analysis of the poles for the kernel function of the Wiener–Hopf equation are presented in Appendix B. Properties of the kernel function which are necessary for its factorisation as a product of two functions, analytic in different halves of the complex plane, are proved in Appendix C. In Appendix D, the derivation of the solution to the Wiener–Hopf equation is given. Finally, asymptotes in the vicinity of the zero wavenumber for the functions obtained after the factorisation of the kernel function are derived in Appendix E.

2. Elastic lattice and the governing equations

2.1. The notion of Slepyan's crack

The crack in the infinite triangular lattice considered here (see Fig. 1), is a semi-infinite fault which appears as the result of subsequent breakage of bonds in a straight line, and propagates with a constant speed V according to $\eta = x - Vt$ (e.g. between rows $n=0$ and -1 in Fig. 1). Here, x is the horizontal coordinate associated with the crack tip node, directed in the line of the propagation of the crack, and t is time. This approach to describing the crack propagation, was first used in Slepyan (2001b). It allows for the reduction of the full transient problem to a simple difference problem in the vertical direction following the Fourier transform with respect to η, where the forces in the bonds of the lattice can be linked to the displacements and stresses through a Wiener–Hopf equation along the crack. Dispersion properties of this lattice configuration can also be obtained through the roots and poles of the kernel function involved this equation. The approach is elegant and leads to a closed form solution. One of the drawbacks is that the model does not serve the case of small crack velocities, as discussed further in the text below. However, for a finite range of values of a subsonic crack speed, one can identify a regime of steady crack propagation. In the real physical situation, crack propagation can be treated in the averaged sense, and the average crack velocity can be evaluated, as discussed in Mishuris et al. (2009a).

2.2. Non-uniform lattice

We consider a triangular lattice containing a semi-infinite crack (see Fig. 1), where horizontal bonds are assumed to have stiffness μ_1 and diagonal bonds stiffness μ_2. In the following, the ratio of bar stiffnesses is $\alpha = \mu_1/\mu_2$. The length of the bonds connecting the particles is normalised to 1. All particles are assumed to have identical mass m.

To characterise the positions of masses within the lattice, it is convenient to use the basis vectors $\mathbf{e}_0 = (1,0)^T$ and $\mathbf{e}_1 = (1/2, \sqrt{3}/2)^T$. The in-plane displacement vector at the node $\mathbf{x} = k\mathbf{e}_0 + n\mathbf{e}_1$, where k,n are integers, is $\mathbf{u}(t,\mathbf{x})$. Projected displacements onto the horizontal and vertical axes, associated with the crack tip node, are denoted by u and v, respectively.

It is also assumed that the external forces $\mathcal{G}$ and $\mathcal{H}$ act on the nodes along $n=0$. Along $n=0$ the forces $\mathcal{G}$ and $\mathcal{H}$ are directed along $-\mathbf{e}_1$ and $\mathbf{e}_0 - \mathbf{e}_1$, respectively (see Fig. 2). The exact form of these forces will be specified in Section 4.

We define the constant

$$C_R = \frac{1}{2m^{1/2}} \sqrt{2\mu_1 + \mu_2 - \sqrt{3\mu_1^2 + (\mu_1 - \mu_2)^2}}, \tag{2.1}$$

as the critical surface wave speed for a wave that propagates along the crack faces aligned with the x-axis, which are traction free. The crack is assumed to propagate steadily through lattice with speed $V \le C_R$, and this propagation is caused by the breaking of the bonds between rows $n=-1$ and $n=0$. Note that for bond length normalised to 1 and $\mu_1 = \mu_2$ the

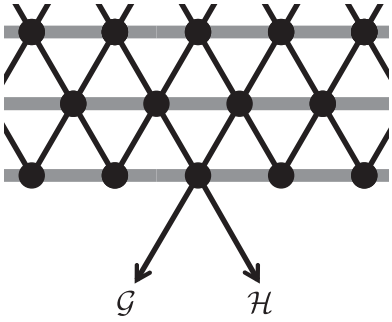

Fig. 2. The particles along the crack face at $n=0$, acted on by external forces $\mathcal{G}$ and $\mathcal{H}$.

above expression coincides with that for the Rayleigh wave speed for the homogeneous infinite triangular lattice with a semi-infinite crack (Slepyan, 2002).

2.3. Normalised crack speed

Let V_* be the dimensionless crack speed defined by $V_* = V\sqrt{m/\mu_2}$. Since we consider the sub-critical surface wave speed regime, using (2.1) we obtain

$$V_*^2 \le g(\alpha) = \frac{C_R^2 m}{\mu_2} = \frac{2\alpha+1-\sqrt{3\alpha^2+(\alpha-1)^2}}{4}. \tag{2.2}$$

Proposition 1. *The function $g(\alpha)$ is increasing for $\alpha > 0$, with $0 < g(\alpha) \le 3/8$ and $dg/d\alpha < 3/4$.*

Proof. For $g(\alpha)$, in (2.2), we have

$$\frac{dg}{d\alpha}(\alpha) = \frac{1}{2} - \frac{4\alpha-1}{4\sqrt{3\alpha^2+(\alpha-1)^2}},$$

and with $0 < \alpha \le 1/4$, it is clear that $g(\alpha)$ is an increasing function on this interval. Now, let $\alpha > 1/4$. Using the inequality

$$3\alpha^2+(\alpha-1)^2 > \frac{(4\alpha-1)^2}{4}, \tag{2.3}$$

leads to

$$\frac{dg}{d\alpha}(\alpha) > 0, \quad \text{for } \alpha > 1/4.$$

Therefore, $g(\alpha)$ is an increasing function for $\alpha > 0$, and

$$g(0) = 0, \quad \text{and} \quad g(\alpha) \le \lim_{\alpha\to\infty} g(\alpha) = \frac{3}{8}, \quad \alpha > 0.$$

Next, owing to (2.3)

$$\frac{d^2g}{d\alpha^2}(\alpha) = \frac{1}{4\sqrt{3\alpha^2+(\alpha-1)^2}}\left(\frac{(1-4\alpha)^2}{3\alpha^2+(\alpha-1)^2} - 4\right) < 0,$$

which shows $dg/d\alpha$ is a decreasing function, that takes its maximum as $\alpha \to 0$

$$\frac{dg}{d\alpha}(0) = \frac{3}{4}. \qquad \square$$

2.4. Dynamic equations for the lattice above the crack

The equations of motion for a particle inside the lattice ($n > 0$) are

$$m\ddot{\mathbf{u}} = \mu_1 \mathbf{e}_0 \cdot \left\{\mathbf{u}|_{\mathbf{x}+\mathbf{e}_0} + \mathbf{u}|_{\mathbf{x}-\mathbf{e}_0} - 2\mathbf{u}|_{\mathbf{x}}\right\}\mathbf{e}_0 + \mu_2 \sum_{j=1,2} \mathbf{v}_j \cdot \left\{\mathbf{u}|_{\mathbf{x}+\mathbf{v}_j} + \mathbf{u}|_{\mathbf{x}-\mathbf{v}_j} - 2\mathbf{u}|_{\mathbf{x}}\right\}\mathbf{v}_j, \tag{2.4}$$

where $\mathbf{v}_1 = \mathbf{e}_1$ and $\mathbf{v}_2 = \mathbf{e}_1 - \mathbf{e}_0$.

Making a change of variable to the moving coordinate system, we set $\eta = x - Vt$. Then (2.4) in terms of projected displacements becomes

$$\begin{aligned}
&\frac{mV^2}{\mu_2}\frac{d^2u}{d\eta^2}(\eta,n) - \frac{1}{4}[u(\eta+1/2,n+1)+u(\eta-1/2,n+1)+u(\eta+1/2,n-1)+u(\eta-1/2,n-1)]\\
&\quad -\frac{\sqrt{3}}{4}[v(\eta+1/2,n+1)-v(\eta-1/2,n+1)+v(\eta-1/2,n-1)-v(\eta+1/2,n-1)]\\
&\quad -\alpha[u(\eta+1,n)+u(\eta-1,n)]+(1+2\alpha)u(\eta,n) = 0,
\end{aligned}$$

and

$$\begin{aligned}
&\frac{mV^2}{\mu_2}\frac{d^2v}{d\eta^2}(\eta,n) - \frac{\sqrt{3}}{4}[u(\eta+1/2,n+1)-u(\eta-1/2,n+1)-u(\eta+1/2,n-1)+u(\eta-1/2,n-1)]\\
&\quad -\frac{3}{4}[v(\eta+1/2,n+1)+v(\eta-1/2,n+1)+v(\eta+1/2,n-1)+v(\eta-1/2,n-1)]+3v(\eta,n) = 0,
\end{aligned}$$

where $u(\eta,n)$ and $v(\eta,n)$ are the horizontal and vertical components, respectively, of the displacement vector $\mathbf{u}$, along row n after the change of variable.

3. Solution for the lattice half-plane

Here, for the intact part of the lattice ($n>0$) we will obtain the solution to the problem of Section 2.4. We follow the method discussed in Slepyan (2001b), which makes use of the continuous Fourier transforms u^F and v^F with respect to the moving coordinate associated with the crack. The Fourier transform is defined as

$$U^F=\int_{-\infty}^{\infty}U(\eta)e^{i\xi\eta}\,d\eta,$$

where the Fourier transform variable ξ represents the wavenumber. We also introduce the left-sided and right-sided Fourier transforms U_- and U_+

$$U_{\pm}=\int_{-\infty}^{\infty}U(\eta)H(\pm\eta)e^{i\xi\eta}\,d\eta,$$

where H is the Heaviside function. When regularisation is needed, ξ is assumed to be complex with $\pm\,\mathrm{Im}\,\xi>0$.

3.1. The continuous Fourier transform of the system

We take the Fourier transform with respect to η, and obtain

$$[u^F(\xi,n+1)+u^F(\xi,n-1)]\cos(\xi/2)-2[1+2\alpha(1-\cos(\xi))+m(\varepsilon+i\xi V)^2/\mu_2]u^F(\xi,n)$$
$$-i\sqrt{3}\sin(\xi/2)[v^F(\xi,n+1)-v^F(\xi,n-1)]=0, \tag{3.1}$$

$$3[v^F(\xi,n+1)+v^F(\xi,n-1)]\cos(\xi/2)-2[3+m(\varepsilon+i\xi V)^2/\mu_2]v^F(\xi,n)$$
$$-i\sqrt{3}\sin(\xi/2)[u^F(\xi,n+1)-u^F(\xi,n-1)]=0, \tag{3.2}$$

where ε is the regularisation parameter, $0<\varepsilon\ll 1$.

3.2. General solution for the half-plane lattice

The functions u^F and v^F are sought in the form

$$u^F=C\Lambda^n \quad\text{and}\quad v^F=D\Lambda^n.$$

Insertion of these into (3.1) and (3.2) yield

$$C\{(\Lambda+1/\Lambda)\cos(\xi/2)-2[1+2\alpha(1-\cos(\xi))+m(\varepsilon+i\xi V)^2/\mu_2]\}-i\sqrt{3}\sin(\xi/2)(\Lambda-1/\Lambda)D=0,$$

$$D\{3(\Lambda+1/\Lambda)\cos(\xi/2)-2(3+m(\varepsilon+i\xi V)^2/\mu_2)\}-i\sqrt{3}\sin(\xi/2)(\Lambda-1/\Lambda)C=0.$$

For non-trivial solutions of C and D, the biquadratic equation in terms of Λ must be satisfied

$$(\Lambda+1/\Lambda)^2-2\left\{2+2\alpha(1-\cos(\xi))+\frac{4}{3\mu_2}m(\varepsilon+i\xi V)^2\right\}(\Lambda+1/\Lambda)\cos(\xi/2)$$
$$+2\{1+\cos(\xi)+4\alpha(1-\cos(\xi))\}+\frac{4}{3\mu_2}m(\varepsilon+i\xi V)^2\left\{4+2\alpha(1-\cos(\xi))+\frac{m}{\mu_2}(\varepsilon+i\xi V)^2\right\}=0. \tag{3.3}$$

We require that $|\Lambda|\le 1$, and this leads to the solutions

$$\Lambda_j=z_j\pm\sqrt{z_j^2-1},\quad j=1,2, \tag{3.4}$$

where the sign in front of the square root in Λ_j has to be chosen so that the condition $|\Lambda_j|\le 1$, $j=1,2$, for $\xi\in\mathbb{R}$ and $V>0$, is satisfied. For $j=1,\,2$

$$z_j=\left(1+2\alpha\sin^2(\xi/2)+\frac{2m(\varepsilon+i\xi V)^2}{3\mu_2}\right)\cos(\xi/2)+(-1)^j\left[\frac{m^2(\varepsilon+i\xi V)^4}{9\mu_2^2}-4\sin^2(\xi/2)\left(\alpha\sin^2(\xi/2)+\frac{m(\varepsilon+i\xi V)^2}{3\mu_2}\right)\right.$$
$$\left.\times\left(\alpha\sin^2(\xi/2)+\frac{m(\varepsilon+i\xi V)^2}{3\mu_2}+1-\alpha\right)\right]^{1/2}. \tag{3.5}$$

Then for $n>0$, with such choices of Λ, the Fourier transforms of the displacements have the form

$$\begin{pmatrix}u^F(\xi,n)\\ v^F(\xi,n)\end{pmatrix}=\frac{1}{f_v(\Lambda_1)f_v(\Lambda_2)}\begin{pmatrix}f_v(\Lambda_1)f_v(\Lambda_2) & f_v(\Lambda_1)f_v(\Lambda_2)\\ -if_u(\Lambda_1)f_v(\Lambda_2) & -if_u(\Lambda_2)f_v(\Lambda_1)\end{pmatrix}\begin{pmatrix}C_1\Lambda_1^n\\ C_2\Lambda_2^n\end{pmatrix}, \tag{3.6}$$

where

$$f_u(\Lambda)=-\sqrt{3}\sin(\xi/2)(\Lambda^2-1)\quad\text{and}\quad f_v(\Lambda)=3(\Lambda^2+1)\cos(\xi/2)-2\Lambda(3+m(\varepsilon+i\xi V)^2/\mu_2),$$

and C_j, $j=1,\,2$ are arbitrary constants, to be determined.

3.3. Mode I symmetry conditions

For Mode I, using the symmetry relations

$$u(\eta,-n-1)=u(\eta,n),\quad v(\eta,-n-1)=-v(\eta,n), \tag{3.7}$$

we can extend the solution in the upper half-plane (3.6) to the lower half-plane. Then, for $n\le -1$, the Fourier transforms of the horizontal and vertical displacements are

$$\begin{pmatrix} u^F(\xi,n)\\ v^F(\xi,n)\end{pmatrix}=\frac{1}{f_v(\Lambda_1)f_v(\Lambda_2)}\begin{pmatrix} f_v(\Lambda_1)f_v(\Lambda_2) & f_v(\Lambda_1)f_v(\Lambda_2)\\ \mathrm{i}f_u(\Lambda_1)f_v(\Lambda_2) & \mathrm{i}f_u(\Lambda_2)f_v(\Lambda_1)\end{pmatrix}\begin{pmatrix} C_1\Lambda_1^{-n-1}\\ C_2\Lambda_2^{-n-1}\end{pmatrix}.$$

The elongations in the bonds directed along $-\mathbf{e}_1$ and $\mathbf{e}_0-\mathbf{e}_1$, respectively, for a node in the upper half-plane of the lattice, have the form

$$\mathcal{S}(\eta,n)=\frac{1}{2}[u(\eta,n)-u(\eta-1/2,n-1)]+\frac{\sqrt{3}}{2}[v(\eta,n)-v(\eta-1/2,n-1)], \tag{3.8}$$

$$\mathcal{T}(\eta,n)=\frac{1}{2}[u(\eta+1/2,n-1)-u(\eta,n)]+\frac{\sqrt{3}}{2}[v(\eta,n)-v(\eta+1/2,n-1)]. \tag{3.9}$$

The symmetry conditions (3.7) lead to

$$\mathcal{S}(\eta,0)=\frac{1}{2}[u(\eta,0)-u(\eta-1/2,0)]+\frac{\sqrt{3}}{2}[v(\eta,0)+v(\eta-1/2,0)],\quad \mathcal{T}(\eta,0)=\mathcal{S}(\eta+1/2,0)$$

or

$$\mathcal{S}^F(\xi,0)=\frac{1}{2}(1-e^{\mathrm{i}\xi/2})u^F(\xi,0)+\frac{\sqrt{3}}{2}(1+e^{\mathrm{i}\xi/2})v^F(\xi,0),\quad \mathcal{T}^F(\xi,0)=\mathcal{S}^F(\xi,0)e^{-\mathrm{i}\xi/2}. \tag{3.10}$$

The representation (3.6), then allows $\mathcal{S}^F$ in (3.10) to be rewritten as

$$\mathcal{S}^F(\xi,0)=\frac{1}{2f_v(\Lambda_1)f_v(\Lambda_2)}\mathbf{R}^T\mathbf{T}\mathbf{B}(\Lambda_1,\Lambda_2)\mathbf{C}, \tag{3.11}$$

with

$$\mathbf{C}=\begin{pmatrix} C_1\\ C_2\end{pmatrix},\quad \mathbf{R}=\begin{pmatrix} 1-e^{\mathrm{i}\xi/2}\\ \mathrm{i}(1+e^{\mathrm{i}\xi/2})\end{pmatrix},$$

and

$$\mathbf{T}=\begin{pmatrix} 1 & 0\\ 0 & \sqrt{3}\end{pmatrix},\quad \mathbf{B}(\Lambda_1,\Lambda_2)=\begin{pmatrix} f_v(\Lambda_1)f_v(\Lambda_2) & f_v(\Lambda_1)f_v(\Lambda_2)\\ -f_u(\Lambda_1)f_v(\Lambda_2) & -f_u(\Lambda_2)f_v(\Lambda_1)\end{pmatrix}.$$

In contrast, if the symmetry relation (3.7) is not used, the Fourier transform with respect to η can be applied directly to (3.8), (3.9)

$$\begin{aligned}\mathcal{S}^F(\xi,n)=&\frac{1}{2f_v(\Lambda_1)f_v(\Lambda_2)}[C_1\Lambda_1^n(1-\Lambda_1^{-1}e^{\mathrm{i}\xi/2})[f_v(\Lambda_1)f_v(\Lambda_2)-\mathrm{i}\sqrt{3}f_u(\Lambda_1)f_v(\Lambda_2)]\\&+C_2\Lambda_2^n(1-\Lambda_2^{-1}e^{\mathrm{i}\xi/2})[f_v(\Lambda_2)f_v(\Lambda_1)-\mathrm{i}\sqrt{3}f_u(\Lambda_2)f_v(\Lambda_1)]],\end{aligned} \tag{3.12}$$

$$\begin{aligned}\mathcal{T}^F(\xi,n)=&-\frac{1}{2f_v(\Lambda_1)f_v(\Lambda_2)}[C_1\Lambda_1^n(1-\Lambda_1^{-1}e^{-\mathrm{i}\xi/2})[f_v(\Lambda_1)f_v(\Lambda_2)+\mathrm{i}\sqrt{3}f_u(\Lambda_1)f_v(\Lambda_2)]\\&+C_2\Lambda_2^n(1-\Lambda_2^{-1}e^{-\mathrm{i}\xi/2})[f_v(\Lambda_2)f_v(\Lambda_1)+\mathrm{i}\sqrt{3}f_u(\Lambda_2)f_v(\Lambda_1)]],\end{aligned} \tag{3.13}$$

where the formulae (3.6) have been used in the derivation. Formally taking the limit as $n\to 0$, we obtain

$$\begin{aligned}\mathcal{P}^F(\xi)=&\frac{1}{2f_v(\Lambda_1)f_v(\Lambda_2)}[C_1(1-\Lambda_1^{-1}e^{\mathrm{i}\xi/2})[f_v(\Lambda_1)f_v(\Lambda_2)-\mathrm{i}\sqrt{3}f_u(\Lambda_1)f_v(\Lambda_2)]\\&+C_2(1-\Lambda_2^{-1}e^{\mathrm{i}\xi/2})[f_v(\Lambda_2)f_v(\Lambda_1)-\mathrm{i}\sqrt{3}f_u(\Lambda_2)f_v(\Lambda_1)]],\end{aligned} \tag{3.14}$$

$$\begin{aligned}\mathcal{Q}^F(\xi)=&-\frac{1}{2f_v(\Lambda_1)f_v(\Lambda_2)}[C_1(1-\Lambda_1^{-1}e^{-\mathrm{i}\xi/2})[f_v(\Lambda_1)f_v(\Lambda_2)+\mathrm{i}\sqrt{3}f_u(\Lambda_1)f_v(\Lambda_2)]\\&+C_2(1-\Lambda_2^{-1}e^{-\mathrm{i}\xi/2})[f_v(\Lambda_2)f_v(\Lambda_1)+\mathrm{i}\sqrt{3}f_u(\Lambda_2)f_v(\Lambda_1)]],\end{aligned} \tag{3.15}$$

The notations $\mathcal{P}^F(\xi)$ and $\mathcal{Q}^F(\xi)$ are used instead of $\mathcal{S}^F(\xi,0)$ and $\mathcal{T}^F(\xi,0)$ in the above formulae.

4. The Wiener–Hopf equation along the crack

In this section, we will use the equations of motion for a particle on the upper crack face ($n=0$), to derive a Wiener–Hopf equation. The kernel function of this equation is also obtained and its properties are investigated. This function is used in (a) Section 5 for analysing the dispersion properties of the lattice and (b) for computing the energy release rate ratio of the propagating crack in Section 7.

4.1. Dynamic equations along the crack face ($n=0$)

Now we consider the equations of motion for particles along $n=0$. The equations are similar to those presented in Section 2.4. However, since particles along the crack face have no bonds corresponding to the vectors $-\mathbf{e}_1$ and $\mathbf{e}_0-\mathbf{e}_1$, and are acted on by external forces $\mathcal{G}$ and $\mathcal{H}$ (see Fig. 2), this should be taken into account. For convenience, it will be assumed that these forces have the form $\mathcal{G}(\eta)=\phi(\eta)$ and $\mathcal{H}(\eta)=\phi(\eta+1/2)$, where ϕ is a function to be chosen at a later stage (see Appendix D).

Ahead of the crack, for particles along $n=0$, the elongation of the bonds corresponding to $\mathbf{e}_0$, $\mathbf{e}_1$, $\mathbf{e}_1-\mathbf{e}_0$ and $-\mathbf{e}_0$ are the same as those for a particle in the intact upper lattice half plane. Also the internal force of the bond in the direction of $-\mathbf{e}_1$, can be written as

$$\mathcal{M}(\eta,0)=\mathcal{S}(\eta,0)H(\eta),\quad \mathcal{M}^F=\mathcal{S}_+, \tag{4.1}$$

where H is the Heaviside function. Using (3.10) and $\mathcal{M}^F$, a similar expression for the internal force in the bond directed along $\mathbf{e}_0-\mathbf{e}_1$ is obtained, $\mathcal{N}^F=\mathcal{S}_+e^{-\mathrm{i}k/2}$.

Then, the Fourier transform of the equations of motion for the particles along the line $n=0$ are

$$\frac{m}{\mu_2}(\varepsilon+\mathrm{i}\xi V)^2u^F(\xi,0)=\frac{1}{2}\cos(\xi/2)u^F(\xi,1)-\{2\alpha(1-\cos(\xi/2))+1/2\}u^F(\xi,0)$$
$$-\frac{\mathrm{i}\sqrt{3}}{2}\sin(\xi/2)v^F(\xi,1)-\frac{1}{2}(1-e^{-\mathrm{i}\xi/2})(\mathcal{S}_++\phi^F/\mu_2),$$

$$\frac{m}{\mu_2}(\varepsilon+\mathrm{i}\xi V)^2v^F(\xi,0)=-\frac{\mathrm{i}\sqrt{3}}{4}\sin(\xi/2)u^F(\xi,1)+\frac{3}{4}\cos(\xi/2)v^F(\xi,1)-\frac{3}{2}v^F(\xi,0)-\frac{\sqrt{3}}{2}(1+e^{-\mathrm{i}\xi/2})(\mathcal{S}_++\phi^F/\mu_2).$$

In order that the expressions (3.6) fulfill these equations, the system

$$\mathcal{Q}^F(\xi)-\mathcal{P}^F(\xi)=-(1-e^{-\mathrm{i}\xi/2})(\mathcal{S}_++\phi^F/\mu_2),\quad \mathcal{Q}^F(\xi)+\mathcal{P}^F(\xi)=(1+e^{-\mathrm{i}\xi/2})(\mathcal{S}_++\phi^F/\mu_2),$$

should be satisfied (see (3.1), (3.2), and (3.12)–(3.15)). Using (3.14) and (3.15) in the above left-hand sides leads to

$$\boldsymbol{\Xi}(\Lambda_1,\Lambda_2)\mathbf{C}=-\Lambda_1\Lambda_2f_v(\Lambda_1)f_v(\Lambda_2)\overline{\mathbf{R}}(\mathcal{S}_++\phi^F/\mu_2),$$

where the matrix $\boldsymbol{\Xi}(\Lambda_1,\Lambda_2)=[\Xi_{ij}(\Lambda_1,\Lambda_2)]_{i,j=1}^2$ has the entries

$$\Xi_{11}(\Lambda_1,\Lambda_2)=\Lambda_2f_v(\Lambda_2)(f_v(\Lambda_1)(\cos(\xi/2)-\Lambda_1)+\sqrt{3}\sin(\xi/2)f_v(\Lambda_1)),$$

$$\Xi_{21}(\Lambda_1,\Lambda_2)=\Lambda_2f_v(\Lambda_2)(-\sqrt{3}f_u(\Lambda_1)(\cos(\xi/2)-\Lambda_1)+f_v(\Lambda_1)\sin(\xi/2)),$$

$$\Xi_{12}(\Lambda_1,\Lambda_2)=\Xi_{11}(\Lambda_2,\Lambda_1)\quad\text{and}\quad\Xi_{22}(\Lambda_1,\Lambda_2)=\Xi_{21}(\Lambda_2,\Lambda_1).$$

Therefore

$$\mathbf{C}=-\Lambda_1\Lambda_2f_v(\Lambda_1)f_v(\Lambda_2)[\boldsymbol{\Xi}(\Lambda_1,\Lambda_2)]^{-1}\overline{\mathbf{R}}(\mathcal{S}_++\phi^F/\mu_2).$$

Combining this with (3.11) yields

$$\mathcal{S}^F(\xi,0)=-\frac{\Lambda_1\Lambda_2}{2\det(\boldsymbol{\Xi}(\Lambda_1,\Lambda_2))}\mathbf{R}^T\boldsymbol{\Omega}(\Lambda_1,\Lambda_2)\overline{\mathbf{R}}(\mathcal{S}_++\phi^F/\mu_2), \tag{4.2}$$

with

$$\boldsymbol{\Omega}(\Lambda_1,\Lambda_2)=\mathbf{T}\mathbf{B}(\Lambda_1,\Lambda_2)\mathrm{adj}(\boldsymbol{\Xi}(\Lambda_1,\Lambda_2)),$$

and

$$\mathrm{adj}(\boldsymbol{\Xi}(\Lambda_1,\Lambda_2))=\begin{pmatrix}\Xi_{21}(\Lambda_2,\Lambda_1) & -\Xi_{11}(\Lambda_2,\Lambda_1)\\ -\Xi_{21}(\Lambda_1,\Lambda_2) & \Xi_{11}(\Lambda_1,\Lambda_2)\end{pmatrix},$$
$$\det(\boldsymbol{\Xi}(\Lambda_1,\Lambda_2))=\Xi_{11}(\Lambda_1,\Lambda_2)\Xi_{21}(\Lambda_2,\Lambda_1)-\Xi_{11}(\Lambda_2,\Lambda_1)\Xi_{21}(\Lambda_1,\Lambda_2). \tag{4.3}$$

Since

$$\mathrm{adj}(\boldsymbol{\Xi}(\Lambda_2,\Lambda_1))=-\begin{pmatrix}0 & 1\\ 1 & 0\end{pmatrix}\mathrm{adj}(\boldsymbol{\Xi}(\Lambda_1,\Lambda_2)),\quad \mathbf{B}(\Lambda_2,\Lambda_1)=\mathbf{B}(\Lambda_1,\Lambda_2)\begin{pmatrix}0 & 1\\ 1 & 0\end{pmatrix},$$

the matrix $\mathbf{\Omega}$ matrix satisfies the relation

$$\mathbf{\Omega}(\Lambda_1,\Lambda_2) = -\mathbf{\Omega}(\Lambda_2,\Lambda_1). \tag{4.4}$$

4.2. The Wiener–Hopf equation

Next we set

$$\mathcal{S}^F(\xi,0) = \mathcal{S}_+ + \mathcal{S}_-,$$

where $\mathcal{S}_+$, $\mathcal{S}_-$ are functions analytic in the upper and lower half-planes of the complex plane, and as in (4.1), $\mathcal{M}^F(\xi,0) = \mathcal{S}_+$, whereas the quantity $\mathcal{S}^F$ satisfies (4.2). After inserting this into (4.2), we obtain an equation of the form

$$L(\varepsilon+\mathrm{i}\xi V,\xi)\mathcal{S}_+ + \mathcal{S}_- = (1-L(\varepsilon+\mathrm{i}\xi V,\xi))\phi^F/\mu_2. \tag{4.5}$$

Here,

$$L(\varepsilon+\mathrm{i}\xi V,\xi) = 1 + \frac{\Lambda_1\Lambda_2}{2\det(\mathbf{\Xi}(\Lambda_1,\Lambda_2))}\mathbf{R}^T\mathbf{\Omega}(\Lambda_1,\Lambda_2)\overline{\mathbf{R}},$$

where Λ_j, $j=1,2$, are given in (3.4).

We note that due to (4.4) and the antisymmetry of $\det(\mathbf{\Xi}(\Lambda_1,\Lambda_2))$ in (4.3) with respect to Λ_1 and Λ_2, that $L(\varepsilon+\mathrm{i}\xi V,\xi)$ is symmetric with respect to Λ_1 and Λ_2. An equivalent representation for $L(\varepsilon+\mathrm{i}\xi V,\xi)$ in terms of z_1 and z_2 (see (3.4) and (3.5)) is given by

$$L(\varepsilon+\mathrm{i}\xi V,\xi) = \frac{3r(\Lambda_1^*)r(\Lambda_2^*)(z_2-z_1)\sqrt{z_1^2-1}\sqrt{z_2^2-1}}{r(\Lambda_1^*)F(z_2)\sqrt{z_1^2-1}-r(\Lambda_2^*)F(z_1)\sqrt{z_2^2-1}}, \tag{4.6}$$

where

$$r(\Lambda) = \begin{cases} 1, & |\Lambda| \le 1, \\ -1, & \text{otherwise}, \end{cases}$$

$$F(z) = 3(\cos(\xi/2)-z)^2 + 6\alpha\sin^2(\xi/2)(1+\cos(\xi/2))(1-z) + \frac{m}{\mu_2}(\varepsilon+\mathrm{i}\xi V)^2[1-z\cos(\xi/2)+(1+\cos(\xi/2))(1-z)].$$

The representation for $L(\varepsilon+\mathrm{i}\xi V,\xi)$ in (4.6), contains the stiffness contrast parameter α which is found in the function F. For the case $\alpha=1$, (4.6) is similar to (12.47) of Slepyan (2002, Section 12.3.5), with the only difference here being that the functions $r(\Lambda_1^*)$, $r(\Lambda_2^*)$ have been included to indicate the change of the branch cuts of the square roots whenever $|\Lambda_{1,2}|>1$.

In the derivation of (4.6), from (3.4) we used

$$\Lambda_j = z_j - r(\Lambda_j^*)\sqrt{z_j^2-1},$$

together with the fact

$$\frac{1}{\Lambda_j} = z_j + r(\Lambda_j^*)\sqrt{z_j^2-1}, \quad \text{for } j=1,2.$$

4.3. Asymptotics of $\Lambda_{1,2}$

Here, we obtain estimates for the behaviour of the roots of (3.3), in the neighbourhood of zero and infinity, and discuss their properties.

For the auxiliary functions z_j, $j=1,2$ we have

$$z_j = \frac{m(\varepsilon+\mathrm{i}\xi V)^2}{3\mu_2}\left[2\cos(\xi/2)+(-1)^j\sqrt{1-4\sin^2(\xi/2)}\right] + O(Y_l), \quad j=1,2, \quad \xi\to\pm\infty, \tag{4.7}$$

where the term in the parenthesis is non-zero for all ξ. Here, $Y_l = O(1)$ for most values of ξ, however for a periodic sequence of $\xi=\xi_l$ we have this is $Y_l = O((\varepsilon+\mathrm{i}\xi V)^{-2})$.

In the other limit, $\xi\to 0$, we obtain

$$z_j = 1 + \frac{1}{24}d_j\xi^2 + O\left(\xi^4\right), \quad \xi\to 0,$$

$$\sqrt{z_j^2-1} = \frac{\sqrt{3}\xi}{6}\sqrt{d_j} + O(|\xi|^3), \quad j=1,2, \tag{4.8}$$

where

$$d_j = 3(4\alpha-1)-16V_*^2+(-1)^j 4M_0, \quad j=1,2, \tag{4.9}$$

$$M_0 = \sqrt{4V_*^4+3(\alpha-1)(3\alpha-4V_*^2)}, \tag{4.10}$$

and $V_* = V\sqrt{m/\mu_2}$, as above.

Now we consider the behaviour of $\Lambda_{1,2}$ at infinity, we have

$$\Lambda_j = \frac{1}{2z_j}+O(|z_j|^{-3}), \quad |\xi|\to\infty, \tag{4.11}$$

that is, $\Lambda_j = O(\xi^{-2})$ as $|\xi|\to\infty$ and here the sign in front of the square root in (3.4) is chosen to maintain the condition $|\Lambda_j|\le 1$, $j=1, 2$, in this limit.

Near zero

$$\Lambda_j = 1 \pm \frac{\sqrt{3}\xi}{6}\sqrt{d_j}+O(\xi^2), \quad \xi\to+0. \tag{4.12}$$

Here, the sign in front of the term linear in ξ is chosen so that $|\Lambda_{1,2}|\le 1$ for $\xi\to 0$. In the next section, we analyse the behaviour of d_j, $j=1, 2$ in (4.9) for $\alpha>0$ and $0<V_*\le C_R(m/\mu_2)^{1/2}$. In particular, we show that d_j, $j=1, 2$, do not belong on the negative real axis. If d_j, $j=1, 2$, is non-negative, then in the above expression the sign "$-$" should be used. For a complex d_j, the sign is chosen in such a way that $|\Lambda_j|\le 1$.

4.4. The constants $d_{1,2}$

Here we show that $d_{1,2}$ do not belong to the negative real axis in the complex plane. The proposition below is proved for d_1 and the result extends to d_2 as well.

Proposition 2. *For $\alpha>0$ and $0<V_*\le C_R(m/\mu_2)^{1/2}$, we have $d_1\in\mathbb{C}\backslash\mathbb{R}_-$.*

Proof. We begin by assuming on the contrary that d_1 is negative, which is equivalent to the inequality

$$3(4\alpha-1)-16V_*^2 < 4\sqrt{4V_*^4+3(\alpha-1)(3\alpha-4V_*^2)}, \tag{4.13}$$

with the assumption that the term under the square root in the right-hand side is positive. This gives rise to the cases:

(a)
$$3(4\alpha-1)-16V_*^2>0,$$
together with
$$(3(4\alpha-1)-16V_*^2)^2 < 16(4V_*^4+3(\alpha-1)(3\alpha-4V_*^2))$$
or

(b)
$$3(4\alpha-1)-16V_*^2<0 \quad \text{and} \quad 4V_*^4+3(\alpha-1)(3\alpha-4V_*^2)>0.$$

The Case (a). One can obtain the inequality

$$V_*^4-\frac{2\alpha+1}{2}V_*^2+\frac{3}{8}\left(\alpha+\frac{1}{8}\right)<0.$$

The quadratic function of V_*^2, in the left-hand side, has the zeros

$$\nu_{1,2}^2 = \frac{3}{8}, \quad \frac{1}{8}+\alpha,$$

which for $\alpha>0$, are both positive. Then (4.13) is only valid if $V_*^2\in(\nu_1^2,\nu_2^2)$ for $\alpha\ge 1/4$ or $V_*^2\in(\nu_2^2,\nu_1^2)$ for $\alpha<1/4$. We now show V_*^2 lies outside these intervals for $\alpha>0$.

By Proposition 1,

$$\max\{V_*^2\} = g(\alpha)\le\nu_1^2, \quad \text{when } \alpha\ge 1/4, \tag{4.14}$$

where $g(\alpha)$ is given in (2.2).

For $\alpha<1/4$, owing again to Proposition 1,

$$\frac{dg}{d\alpha}(\alpha)<\frac{3}{4}, \quad \text{for} \quad \alpha>0, \quad g(0)<\frac{1}{8}, \quad \text{and} \quad g(1/4)=\frac{3}{8}\left(1-\frac{\sqrt{3}}{3}\right)<\frac{3}{8}.$$

Thus

$$\max\{V_*^2\} = g(\alpha) < v_2^2, \quad \text{when } 0<\alpha<1/4.$$

This inequality with (4.14) shows that (4.13) is not valid for $V_* \in (0, C_R\sqrt{m/\mu_2}]$ and $\alpha>0$ for case (a) above.

The Case (b). The second inequality of this case can be rewritten as

$$V_*^4 + 3(1-\alpha)V_*^2 - \frac{9\alpha(1-\alpha)}{4} > 0, \tag{4.15}$$

where now the quadratic function on the left-hand side has zeros

$$w_\pm^2 = \frac{3}{2}[\alpha - 1 \pm \sqrt{1-\alpha}].$$

When $\alpha \geq 1$ the inequality (4.15) is satisfied (since the zeros of the left-hand side are complex), and it remains to show that the inequalities

$$V_*^2 \leq \frac{C_R^2 m}{\mu_2} \quad \text{and} \quad V_*^2 > \frac{3(4\alpha-1)}{16}, \tag{4.16}$$

do not hold. These lead to

$$\frac{3(4\alpha-1)}{16} < g(\alpha), \quad \text{or } \sqrt{3\alpha^2+(\alpha-1)^2} < \frac{7}{4} - \alpha,$$

where the definition of $g(\alpha)$ in (2.2) has been used. From the above inequalities, we have a contradiction to (4.16) for $\alpha \geq 7/4$. Assume $1 \leq \alpha < 7/4$, then the last inequality leads to

$$\alpha^2 + \frac{1}{2}\alpha - \frac{11}{16} < 0.$$

This is valid for $\alpha \in (0, (-1/2+\sqrt{3})/2)$. Hence (4.13) does not hold.

When $\alpha<1$, for (4.15) to be satisfied we put

$$V_*^2 > w_+^2 = \frac{3}{2}[\alpha - 1 + \sqrt{1-\alpha}],$$

where

$$V_*^2 \leq \frac{C_R^2 m}{\mu_2}, \quad \text{and} \quad V_*^2 > \frac{3(4\alpha-1)}{16}.$$

Here, as before, the last two inequalities are valid if $0<\alpha<(-1/2+\sqrt{3})/2$. It remains to check that

$$V_*^2 > w_+^2 = \frac{3}{2}[\alpha - 1 + \sqrt{1-\alpha}] \quad \text{and} \quad V_*^2 \leq \frac{C_R^2 m}{\mu_2}. \tag{4.17}$$

Both of these yield the inequality

$$\alpha^2\left(\alpha^2 + \alpha - \frac{7}{4}\right) > 0.$$

This is valid for $\alpha > -1/2+\sqrt{2}$ and, since we have assumed that $0<\alpha<(-1/2+\sqrt{3})/2$, we have a contradiction to (4.17). Therefore, (4.13) is not valid for $V_* \in (0, C_R(m/\mu_2)^{1/2}]$ and $\alpha>0$ in case (b) above. □

4.4.1. Asymptotes of $L(\varepsilon+\mathrm{i}\xi V,\xi)$

Here, we obtain the asymptotics of $L(\varepsilon+\mathrm{i}\xi V,\xi)$ for $\xi \to 0$.

Proposition 3. *For $\xi \to 0$, we have*

$$L(\varepsilon+\mathrm{i}\xi V,\xi) \sim L_0 \frac{1}{\sqrt{(\varepsilon+\mathrm{i}\xi)(\varepsilon-\mathrm{i}\xi)}} + O(|\xi|), \qquad \varepsilon \to +0, \tag{4.18}$$

where

$$L_0 = \frac{3\sqrt{d_1 d_2}(B_2\sqrt{d_1}+B_1\sqrt{d_2})}{2\sqrt{3}(3-8V_*^2)(2V_*^2-3\alpha)(V_*^4-\frac{1}{2}(2\alpha+1)V_*^2+\frac{3\alpha}{8})}, \tag{4.19}$$

and

$$B_j = \frac{1}{2}\left[\frac{1}{6}(V_*^2-(-1)^j M_0)^2 - V_*^2\left(\frac{3V_*^2}{2}+1\right) - \frac{3\alpha}{2}\left(\alpha - \frac{1}{2} - 2V_*^2\right)\right], \quad j=1,2. \tag{4.20}$$

Proof. Using (4.8), for $\xi \to 0$

$$z_2 - z_1 = \frac{M_0 \xi^2}{3} + O(\xi^4), \tag{4.21}$$

and

$$F(z_j) = B_j \xi^4 + O(\xi^6), \quad j = 1,2,$$

together with (4.6), (4.9), (4.10) and (4.21) gives (4.18) where

$$L_0 = \frac{M_0 \sqrt{d_1 d_2}}{2\sqrt{3}(B_2\sqrt{d_1} - B_1\sqrt{d_2})}.$$

Multiplying the numerator and the denominator by $B_2\sqrt{d_1} + B_1\sqrt{d_2}$, we arrive at (4.19). □

It is shown in Appendix A that L_0 is positive for $\alpha > 0$, and $V \le C_R$.

5. Roots and poles of the kernel function *L*

Having obtained the expression for the kernel function L, we can now derive expressions for the dispersion relations of the inhomogeneous lattice. We also show that these relations can be used to predict the behaviour of the argument of the function L, which is needed in the computation of the energy release rate ratio for the propagating crack in Section 7. Let $m = 1$,

$$p = 3r(\Lambda_1^*) r(\Lambda_2^*) \sqrt{z_1^2 - 1}\sqrt{z_2^2 - 1}$$

and

$$q = \frac{r(\Lambda_1^*) F(z_2)\sqrt{z_1^2 - 1} - r(\Lambda_2^*) F(z_1)\sqrt{z_2^2 - 1}}{z_2 - z_1}, \tag{5.1}$$

so that in (4.6)

$$L = \frac{p}{q}.$$

We now investigate the zeros of p and q of the above expression. This is carried out by setting $\varepsilon = 0$ and $\Omega = \xi V$, then solving the equations $p = 0$ and $q = 0$ for Ω.

The roots of the equation $p = 0$ are given by

$$\Omega_1^{(N)}(\xi) = \sqrt{6\mu_2}\,|\cos(\xi/4)|, \tag{5.2}$$

$$\Omega_2^{(N)}(\xi) = [2\mu_2 \sin^2(\xi/4) + 4\mu_1 \sin^2(\xi/2)]^{1/2}, \tag{5.3}$$

$$\Omega_3^{(N)}(\xi) = \sqrt{6\mu_2}\,|\sin(\xi/4)|, \tag{5.4}$$

$$\Omega_4^{(N)}(\xi) = [2\mu_2 \cos^2(\xi/4) + 4\mu_1 \sin^2(\xi/2)]^{1/2}. \tag{5.5}$$

Next we obtain the roots of the equation $q = 0$. This equation, after multiplication by

$$r(\Lambda_2^*) F(z_2)\sqrt{z_1^2 - 1} + r(\Lambda_1^*) F(z_1)\sqrt{z_2^2 - 1},$$

leads to

$$\frac{F(z_2)^2(z_1^2 - 1) - F(z_1)^2(z_2^2 - 1)}{(z_2 - z_1)} = 0. \tag{5.6}$$

Solutions of this extended equation are then (5.4), (5.5) and

$$\Omega_1^{(D)}(\xi) = \sqrt{2\mu_1 + \mu_2 - \sqrt{3\mu_1^2 + (\mu_1 - \mu_2)^2}}\,|\sin(\xi/2)|, \tag{5.7}$$

$$\Omega_2^{(D)}(\xi) = \sqrt{6\mu_1}\,|\sin(\xi/2)|, \tag{5.8}$$

$$\Omega_3^{(D)}(\xi) = \sqrt{2\mu_1 + \mu_2 + \sqrt{3\mu_1^2 + (\mu_1 - \mu_2)^2}}\,|\sin(\xi/2)|, \tag{5.9}$$

and it remains to determine which of the roots of (5.6) are those of (5.1). Each dispersion relation satisfies $\Omega(\xi + 4\pi) = \Omega(\xi)$. Also note that for $m = 1$, $\lim_{\xi \to +0} d\Omega_1^{(D)}(\xi)/d\xi$ coincides with (2.1).

Functions (5.4) and (5.5), which are also roots of Eq. (5.1), and are in fact removable singularities of L.

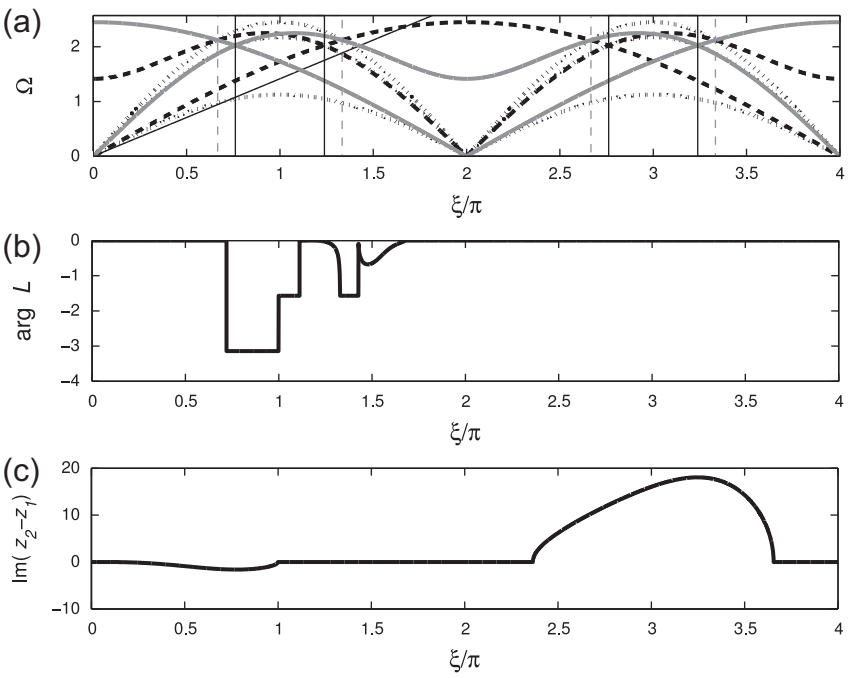

Fig. 3. For $\mu_1=\mu_2=1$, $\alpha=1$, figure (a) shows the dispersion relations (5.2)–(5.5) and (5.7)–(5.9), along with the ray $\Omega=\xi V$ for $V=0.4504$. The roots of L are given by the solid curves, poles are shown by curves with the small dashes and the removable singularities are given by the dashed curves. The regions given in (5.10) and (5.11) where $\Omega_2^{(D)}$ and $\Omega_3^{(D)}$ are roots of $q=0$ are marked by the dashed and solid vertical lines. For comparison, we give the plot of (b) arg(L), and (c) the imaginary part of the factor z_2-z_1 contained in the representation (4.6) of L.

The choice of α and ξ determines when (5.7)–(5.9) are solutions of $q=0$. Here, we present the results for the case $\alpha=1$ and give the description of the behaviour of the argument of L. The function $\Omega_1^{(D)}$ is a solution of (5.1). When

$$0.6667\le\xi/\pi\le 1.3333 \quad \text{and} \quad 2.6667\le\xi/\pi\le 3.3333, \tag{5.10}$$

we have $\Omega_2^{(D)}$ is a solution of $q=0$. For ξ/π satisfying

$$0.7614\le\xi/\pi\le 1.2386 \quad \text{and} \quad 2.7614\le\xi/\pi\le 3.2386, \tag{5.11}$$

$\Omega_3^{(D)}$ is a solution of $q=0$. The inequalities (5.10) and (5.11) are discussed in Appendix B.

In Fig. 3(a) we plot the dispersion relations (5.2)–(5.5) and (5.7)–(5.9), as functions of the wavenumber ξ, for $\mu_1=\mu_2=1$. Included in this figure is the ray $\Omega=V\xi$ corresponding to the speed $V=0.4504$. By comparison with the diagram of arg(L) in Fig. 3(b), we see each intersection of the ray ξV with the dispersion curves corresponds to a jump in arg(L).

At approximately $\xi=\pi$, we have an additional jump in arg(L). This is a result of the behaviour of the factor z_2-z_1 contained in L (see (3.4) and (4.6)). This factor, as shown in Fig. 3(c), is either real or purely imaginary. As we approach $\xi=\pi$, this factor moves from the negative imaginary axis in the complex plane, to the positive real axis (note that z_2-z_1 is the radical function of (3.5) where the positive square root is taken). The corresponding effect is a jump in arg(L) of $\pi/2$.

For a lower crack speed, $V=0.2140$, we present the dispersion diagram along with the ray ξV in Fig. 4(a). On the corresponding picture for arg(L) in Fig. 4(b), we see this function jumps when the ray intersects the dispersion curves. In particular, the ray ξV intersects the curve corresponding to $\Omega_3^{(D)}$ in the second region of (5.11), which again results in a change in the value of arg(L). Also, in Fig. 4(c), at approximately, $\xi=3.4\pi$, we observe that the factor z_2-z_1 moves from the positive real axis to the positive imaginary axis. Again, the result we observe is a jump of $\pi/2$ in arg(L) at this point.

Finally, for $\mu_1=1$ and $\mu_2=10$, ($\alpha=0.1$), $V=0.7998$ we present the dispersion relations, the plot of arg(L) and the imaginary part of the factor z_2-z_1, in Fig. 5(a)–(c). Comparing with Fig. 3, we see the distance between the dispersion curves along with their height has increased, which can lead to greater absolute value of the area under the curve traced by the argument of L.

6. Solution of the Wiener–Hopf equation

6.1. Factorisation of the Wiener–Hopf equation (4.5)

Here, we use the solution presented in Slepyan (2002) and extend it to the situation when the bonds within the lattice have a contrast in stiffness in the principal lattice directions. We define the class $\mathcal{J}$ as the set of complex valued functions

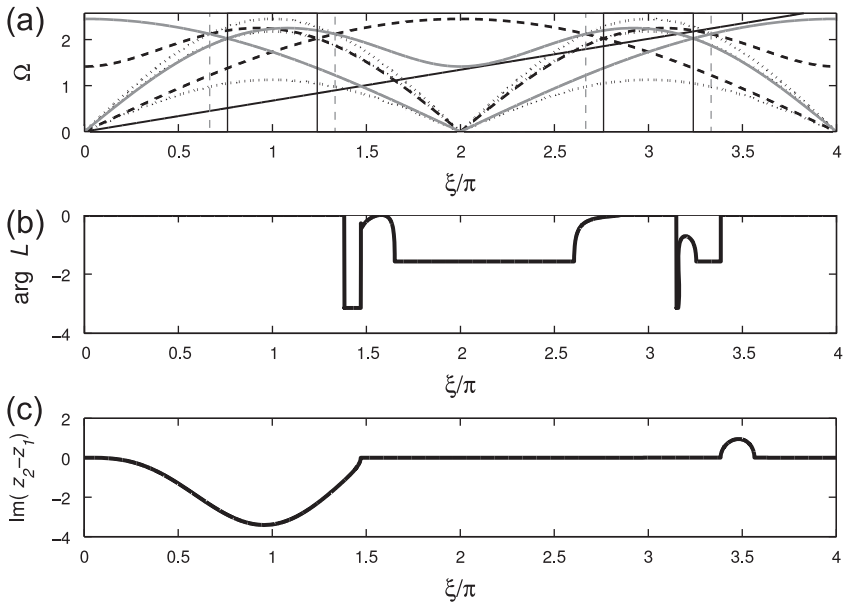

Fig. 4. For $\mu_1=\mu_2=1$, $\alpha=1$, in figure (a) we show the dispersion relations (5.2)–(5.5) and (5.7)–(5.9), along with the ray $\Omega=\xi V$ for $V=0.2140$. The description of the curves in the dispersion diagram is the same as in Fig. 3. We again give the plot of (b) arg(L) and (c) the function Im(z_2-z_1), for the purpose of comparison.

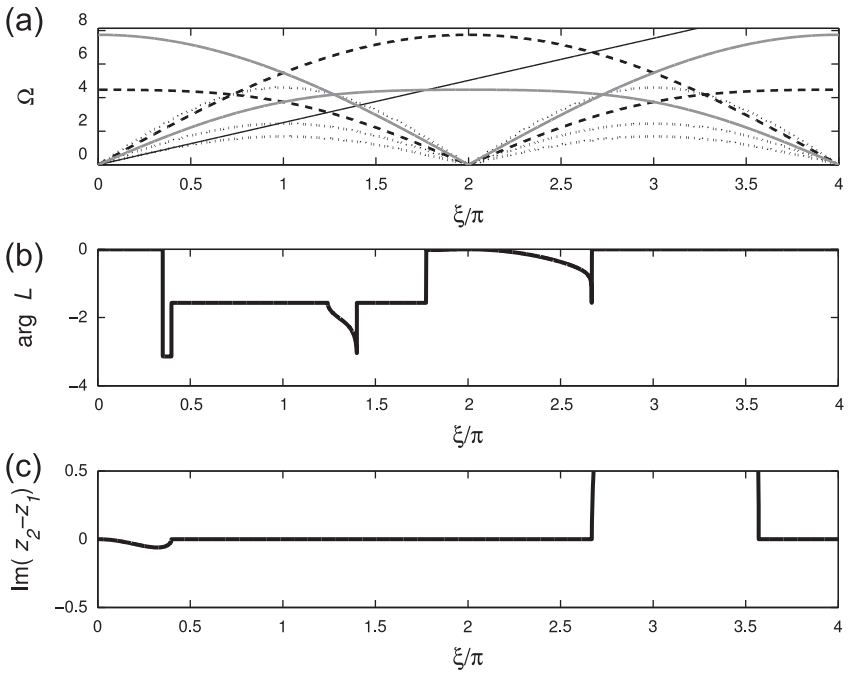

Fig. 5. (a) For $\mu_1=1$, $\mu_2=10$, $\alpha=0.1$, we plot the dispersion relations (5.2)–(5.5) and (5.7)–(5.9), along with the ray $\Omega=\xi V$ for $V=0.7998$. The description of the dispersion curves is given in Fig. 3. The plots of (b) arg(L) and (c) Im(z_2-z_1) are also presented.

$f:\mathbb{R}\to\mathbb{C}$ satisfying

$$\mathrm{Re}(f(\xi))=\mathrm{Re}(f(-\xi)),\quad \mathrm{Im}\,(f(\xi))=-\mathrm{Im}(f(-\xi)).$$

For $\varepsilon>0$, the kernel $L\in\mathcal{J}$ and satisfies

$$\begin{aligned}&\mathrm{Ind}(L(\varepsilon+\mathrm{i}\xi V,\xi))=\lim_{\xi\to\infty}\frac{1}{2\pi}[\arg(L(\varepsilon+\mathrm{i}\xi V,\xi))-\arg(L(\varepsilon-\mathrm{i}\xi V,-\xi))]=0,\\&\arg(L(\varepsilon+\mathrm{i}\xi V,\xi))=-\arg(L(\varepsilon-\mathrm{i}\xi V,-\xi))\quad\text{and}\quad\lim_{\xi\to\pm\infty}L(\varepsilon+\mathrm{i}\xi V,\xi)=1,\end{aligned}\tag{6.1}$$

where $\mathrm{Ind}(L(\varepsilon+\mathrm{i}\xi V,\xi))$ represents the number of times the contour traced by $L(\varepsilon+\mathrm{i}\xi V,\xi)$ in the complex plane winds around the origin. The proofs of these properties are given in Appendix C.

Then, the above conditions allow $L(\varepsilon+\mathrm{i}\xi V,\xi)$ to be factorised in the form

$$L = L_+ L_-,$$

where

$$L_\pm(\varepsilon+\mathrm{i}\xi V,\xi) = \exp\left(\pm\frac{1}{2\pi\mathrm{i}}\int_{-\infty}^{\infty}\frac{\ln L(\varepsilon+\mathrm{i}sV,s)}{s-\xi}\,ds\right), \tag{6.2}$$

with $\varepsilon\to+0$, $\mathrm{Im}\,\xi>0$ for L_+ and $\mathrm{Im}\,\xi<0$ for L_-.

The function L_+ (L_-) is an analytic function of ξ in the upper (lower) half of the complex plane. The introduction of the small positive parameter ε into L, shifts its zeros and poles (located on the real axis) into the upper or lower half of the complex plane. Following this shift, the dispersion curves, discussed in Section 5, can be then used to identify in which half plane each root and pole is located (see Slepyan, 2002, Chapter 2).

Suppose ξ_z and ξ_p are wavenumbers which correspond to the intersection of $\Omega=\xi V$ with the zeros and poles of L, respectively (see (5.2)–(5.5) and (5.7)–(5.9)), on the dispersion diagram. Also at these intersection points, let $V<V_g$, where $V_g=d\Omega/d\xi$ is the group velocity. Then, in this case ξ_z and ξ_p will be located in the lower half plane after the introduction of ε in L. Similarly, if $V>V_g$ then ξ_z and ξ_p are shifted into the upper half of the complex plane (see Slepyan, 2002, Section 3.3.3). It is noted that the case $V=V_g$ is not considered here.

From the definition (6.2), it follows that L_+ (L_-) contains all singular and zero points of L which are located in the lower (upper) half of the complex plane for $\varepsilon>0$.

Using (6.1), Eq. (4.5) can then be written as

$$L_+\mathcal{S}_+ + \frac{\mathcal{S}_-}{L_-} = \left(\frac{1}{L_-}-L_+\right)\frac{\phi^F}{\mu_2}, \tag{6.3}$$

which is similar to (12.58) of Slepyan (2002).

Here, the left-hand side of (6.3) is the sum of two analytic functions, one analytic in the upper half of the complex plane, the other analytic in the lower half of the complex plane and in order to solve the problem, we must separate the terms in the right-hand side in the same way. This is carried out by introducing the load ϕ in such a way that it allows for this additive split. In Appendix D, an outline for this procedure is presented for the case when the load ϕ is chosen so that the right-hand side can be represented as a linear combination of Dirac delta functions.

In what follows, we will consider the situation when the load applied along the crack faces generates a term of the form $\mathcal{C}\delta(\xi)$, in the right-hand side of (6.3) (see Appendix D for the derivation). Here, $\mathcal{C}$ is a constant which represents the intensity of the load. Then $\mathcal{S}_+$ and $\mathcal{S}_-$ have the form

$$\mathcal{S}_+ = \frac{\mathcal{C}}{\mu_2 L_+(\varepsilon+\mathrm{i}\xi V,\xi)(\varepsilon-\mathrm{i}\xi)},\quad \mathcal{S}_- = \frac{L_-(\varepsilon+\mathrm{i}\xi V,\xi)\mathcal{C}}{\mu_2(\varepsilon+\mathrm{i}\xi)},\quad \varepsilon\to+0. \tag{6.4}$$

7. Energy release rate ratio

Here, we investigate the dependence of energy release rate ratio (Slepyan, 2002) on the stiffness contrast parameter α. This is defined as

$$\frac{G_0}{G} = \exp\left(\frac{2}{\pi}\int_0^{\infty}\frac{\arg(L(\varepsilon+\mathrm{i}sV,s))}{s}\,ds\right),\quad \varepsilon\to+0, \tag{7.1}$$

where G_0 is the local energy release rate for the semi-infinite crack propagating through the lattice with speed V for sub-critical surface wave speed regime and G is global energy release rate for the crack propagating through the corresponding homogenised medium. This ratio describes the dissipation of energy created by breaking bonds at the crack front.

Next we show (7.1) can be obtained from (6.4). However, we note that the derivation of (7.1) does not depend on the solution of the Wiener–Hopf equation in the previous section. The definitions of G and G_0 follow Slepyan (2002, Chapter 12) as the energy release rates globally and locally respectively. In particular, as in Slepyan (2002), G can be defined as a limit

$$G = \lim_{k\to 0} k^2\mu_2\mathcal{S}_-(-\mathrm{i}k)\mathcal{S}_+(\mathrm{i}k),$$

and the local energy release rate is given as

$$G_0 = \lim_{k\to+\infty} k^2\mu_2\mathcal{S}_-(-\mathrm{i}k)\mathcal{S}_+(\mathrm{i}k).$$

The global energy release rate G follows from the asymptotes of $\mathcal{S}_{\pm}$ as $\xi\to 0$. The asymptotes of $L_{\pm}$ are

$$L_+(\varepsilon+\mathrm{i}\xi V,\xi)\sim\frac{\sqrt{L_0}}{\sqrt{\varepsilon-\mathrm{i}\xi}}\exp\left(\frac{1}{\pi}\int_0^\infty\frac{\arg(L(\varepsilon+\mathrm{i}sV,s))}{s}\,ds\right),$$
$$L_-(\varepsilon+\mathrm{i}\xi V,\xi)\sim\frac{\sqrt{L_0}}{\sqrt{\varepsilon+\mathrm{i}\xi}}\exp\left(-\frac{1}{\pi}\int_0^\infty\frac{\arg(L(\varepsilon+\mathrm{i}sV,s))}{s}\,ds\right), \tag{7.2}$$

for $\varepsilon\to+0$, and their derivations are found in Appendix E.

Then, owing to (6.4) and (7.2),

$$\mathcal{S}_+\sim\frac{\mathcal{C}}{\mu_2\sqrt{L_0}\sqrt{\varepsilon-\mathrm{i}\xi}}\exp\left(-\frac{1}{\pi}\int_0^\infty\frac{\arg(L(\varepsilon+\mathrm{i}sV,s))}{s}\,ds\right), \tag{7.3}$$

$$\mathcal{S}_-\sim\frac{\sqrt{L_0}\mathcal{C}}{\mu_2(\varepsilon+\mathrm{i}\xi)^{3/2}}\exp\left(-\frac{1}{\pi}\int_0^\infty\frac{\arg(L(\varepsilon+\mathrm{i}sV,s))}{s}\,ds\right),$$

where $\xi\to 0$, $\varepsilon\to+0$, and so

$$G=\frac{\mathcal{C}^2}{\mu_2}\exp\left(-\frac{2}{\pi}\int_0^\infty\frac{\arg(L(\varepsilon+\mathrm{i}sV,s))}{s}\,ds\right),\quad \varepsilon\to+0. \tag{7.4}$$

The local energy release rate is then given by the asymptotes of $\mathcal{S}_{\pm}$ when $\xi\to\infty$. As a result of (6.1) and (6.2), $L_{\pm}\to 1$ as $\xi\to\infty$. In the same limit we have

$$\mathcal{S}_+\sim\frac{\mathcal{C}}{\mu_2(\varepsilon-\mathrm{i}\xi)},\quad \mathcal{S}_-\sim\frac{\mathcal{C}}{\mu_2(\varepsilon+\mathrm{i}\xi)},\quad \xi\to\infty,\ \varepsilon\to+0,$$

and so $\mu_2 G_0=\mathcal{C}^2$. Then this and (7.4) imply (7.1).

7.1. Sensitivity of the energy release rate ratio to the stiffness contrast

In this section, we set $m=\mu_1=1$, so that $\alpha=1/\mu_2$, and we investigate the behaviour of the energy release rate ratio (7.1) as a function of crack speed, when the stiffness ratio is increased (which corresponds to the decrease in the stiffness of the inclined bars). The critical crack speed $C_R(\alpha)$, in this example, has the form (see (2.1))

$$C_R(\alpha)\big|_{m=1,\mu_1=1}=\frac{1}{2\alpha^{1/2}}\sqrt{2\alpha+1-\sqrt{3\alpha^2+(\alpha-1)^2}}. \tag{7.5}$$

The critical surface wave speed $C_R(\alpha)$ is decreasing monotonically as α increases. The upper bound of this function is $C_R(0)=\sqrt{3}/2$ (when the inclined bars are rigid), and for α tending to infinity (the inclined bars are becoming much more softer compared to the horizontal bars) the speed $C_R(\alpha)$ tends to zero. In Fig. 6(a), we plot the energy release rate ratio as a function of normalised crack speed $V/C_R(\alpha)$, for $\alpha=0.05$, 0.1, 0.2, 1, 100. The crack, for low speeds, does not propagate steadily. The intrinsic feature of the model discussed here is that the crack propagates uniformly with speed V. If this assumption is not satisfied then the model does not describe accurately the propagation of the crack, which is depicted by the non-smooth part of the curves on Fig. 6(a), e.g. for approximately $V/C_R(\alpha)<0.5$ when $\alpha=1$. Formally, the oscillations of G_0/G for low values of V/C_R in Fig. 7, are caused by the highly oscillatory behaviour of $\arg(L)$ for low crack speeds, in (7.1), as observed in Section 5. From Fig. 6(a), we see the percentage of speeds less then $C_R(\alpha)$, where this region is located, is decreasing as α is increasing. The proposed model does not describe a true physical behaviour of the lattice system with a crack for low values of V/C_R.

Contained in Fig. 6(b), is the plot of the energy release rate ratio against the crack speed which has been normalised by $C_R(0)=\sqrt{3}/2$. For $\alpha\geq 0.05$ the ratio G_0/G tends to zero as we approach critical speed $C_R(\alpha)$ predicted by (7.5). For $\alpha>0.1$, in the region of instability, the ratio G_0/G increases until it reaches a speed where there is a global maximum. For speeds greater than this, we observe the ratio follows a smooth curve as it decreases to zero at the critical surface wave speed (7.5). In this region, this behaviour shows that the model describes the steady propagation of the semi-infinite crack through the inhomogeneous lattice.

In Mishuris et al. (2009b), the dynamic problem for the propagation of a crack situated in a square-cell lattice, whose rows contain particles of contrasting mass, is discussed. The sensitivity to the contrast in mass, of the ratio of the local energy release rate G_0 (for the lattice) to the global energy release rate G (for the corresponding homogenised material) was also investigated. It was seen the values of G_0/G, for high crack speeds, increased monotonically as the contrast in mass was reduced. Here, as shown in Figs. 6(a), (b) and 7, we do not have any monotonicity in the behaviour of G_0/G for different α. For example, in Fig. 6(a), the curve for $\alpha=0.2$ intersects those for $\alpha=1$,100 at approximately $V/C_R(\alpha)=0.83$ (where we are in the region of stability for all these curves). For speeds higher than this value, the ratio of G_0/G for $\alpha=0.2$ is greater than that for $\alpha=1$ and $\alpha=100$. Another example of this can be seen for the curve corresponding to $\alpha=0.1$.

It was also observed in Mishuris et al. (2009b), for low crack speeds corresponding to the instability region of the model, the values of G_0/G where not monotonic as a function of the mass contrast parameter. A similar feature is also observed here for low crack speeds as the stiffness contrast parameter α is varied. In Fig. 7, we plot the energy release rate ratio for $\alpha=0.9$,1 and 1.1. For speeds $V/C_R(\alpha)<0.5$ (the region of instability), there exists regions where all curves are

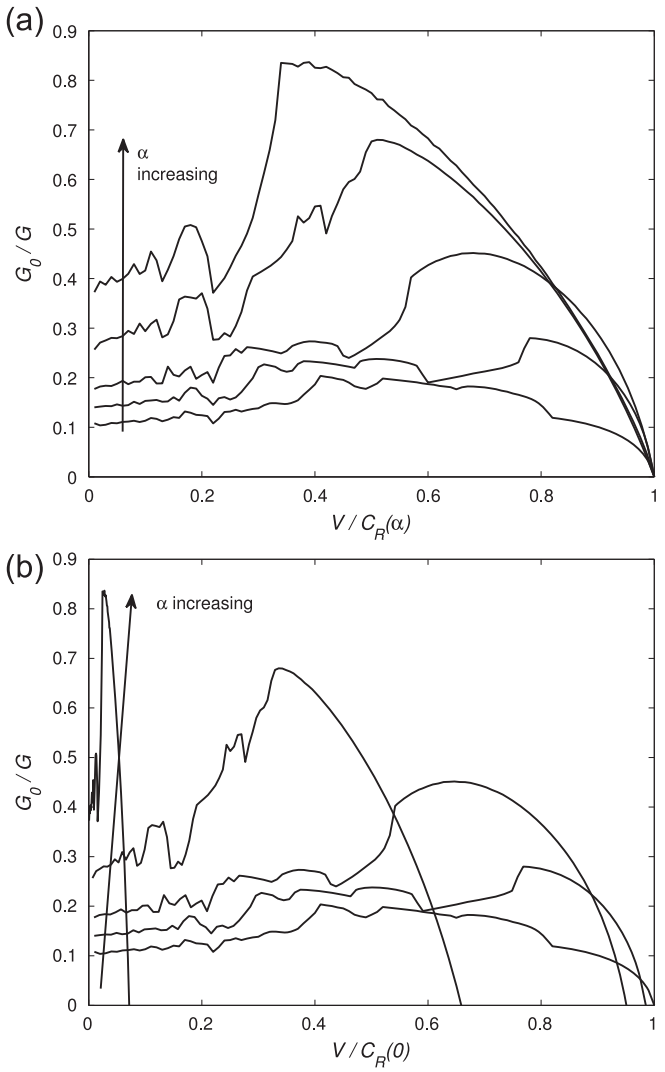

Fig. 6. (a) The energy release rate ratio as a function of the normalised speed $V/C_R(\alpha)$, based on formula (7.1). (b) The ratio G_0/G as a function of the crack speed normalised by the supremum of $C_R(\alpha)$ over $\alpha > 0$ ($C_R(0) = \sqrt{3}/2$). We show the behaviour of this ratio for the stiffness contrasts $\alpha = 0.05, 0.1, 0.2, 1,$ and 100.

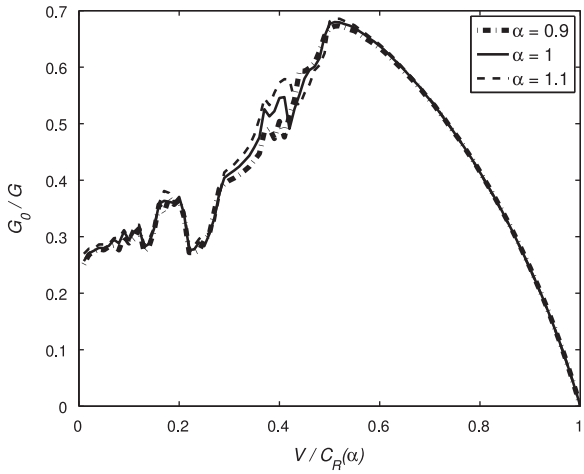

Fig. 7. The energy release rate ratio as a function of the normalised speed $V/C_R(\alpha)$, computed using formula (7.1), for the values $\alpha = 0.9, 1$ and 1.1.

intersecting one another and overlapping. For instance, when $0.35 < V/C_R(\alpha) < 0.5$, again there is no monotonicity in the behaviour of G_0/G as α varies. We note that the critical speed in the scalar case (Mishuris et al., 2009b) was a material constant and did not depend on the contrast ratio.

8. Stress intensity factor in the homogenisation approximation

In this section, we derive the expression for the Mode I stress intensity factor for the semi-infinite crack in the case when the load ϕ applied along the crack faces generates the term $\mathcal{C}\delta(\xi)$ in the right-hand side of (6.3), with $\mathcal{C}$ being the load intensity. The solution of this problem is given in (6.4).

Using the fact that the energy required to break the crack front bond $\mu_2 G_0 = \mathcal{C}^2$ (see the previous section), we compute the inverse Fourier transform of $\mathcal{S}_+$ in (7.3), so that to leading order

$$\mathcal{S}(\eta) \sim \sqrt{\frac{G_0}{\mu_2 L_0 \pi \eta}} \exp\left(-\frac{1}{\pi}\int_0^\infty \frac{\arg(L(\varepsilon + isV,s))}{s}\, ds\right), \quad \text{for } \eta > 0, \tag{8.1}$$

which depends on α and here L_0 is given in Proposition 3. Here, the expression $\mu_2\mathcal{S}(\eta)$ represents the tensile force in the inclined bonds ahead of the crack. Let the normal traction ahead of the crack be σ, then

$$\sigma \sim \sqrt{\frac{3\mu_2 G_0}{L_0 \pi \eta}} \exp\left(-\frac{1}{\pi}\int_0^\infty \frac{\arg(L(\varepsilon + isV,s))}{s}\, ds\right). \tag{8.2}$$

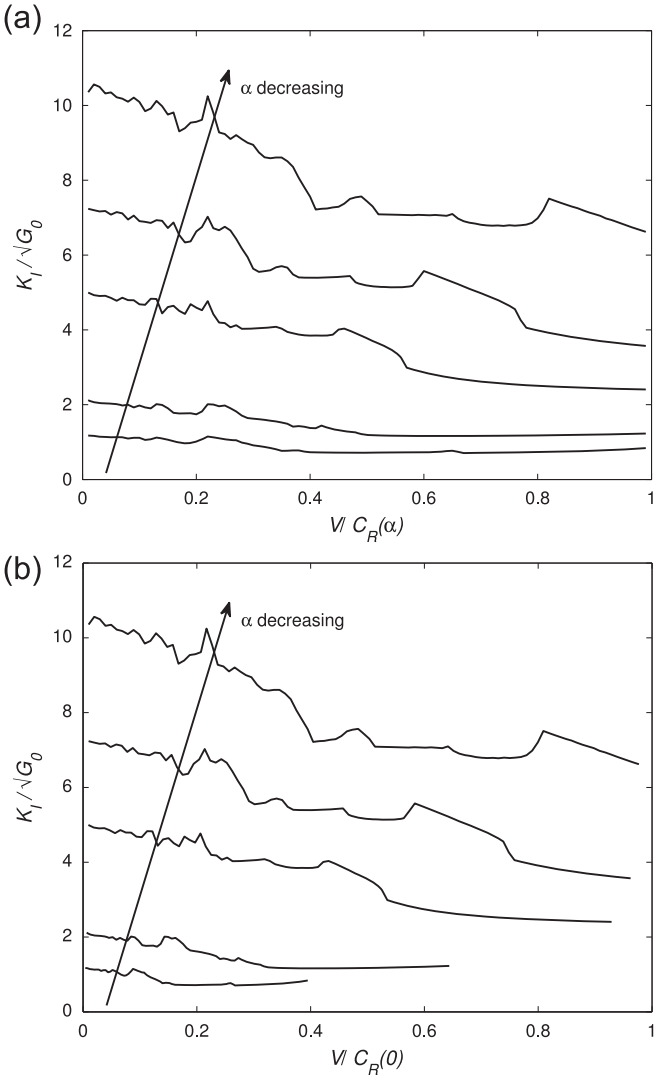

Fig. 8. The normalised stress intensity factor $K_I/\sqrt{G_0}$ as a function of (a) the normalised crack speed $V/C_R(\alpha)$ and (b) the normalised crack speed $V/C_R(0)$, based on formula (8.4), for $\alpha = 0.05, 0.1, 0.2, 1, 3$. Here $C_R(0) = \sqrt{3}/2$ is the supremum of (7.5) for $\alpha > 0$.

The Mode I stress intensity factor K_I, in the far-field is defined by the formula

$$K_I = \lim_{\eta \to +0} \sqrt{2\pi\eta}\sigma. \tag{8.3}$$

On comparison of (8.2) and (8.3), we have the stress intensity factor K_I is

$$K_I(\alpha) = \sqrt{\frac{6\mu_2 G_0}{L_0}} \exp\left(-\frac{1}{\pi}\int_0^\infty \frac{\arg(L(\varepsilon+isV,s))}{s}\, ds\right). \tag{8.4}$$

Now, setting $\mu_1 = 1$ and allowing μ_2 to vary, we investigate the behaviour of K_I as a function of V and α. The expression for $K_I/\sqrt{G_0}$ is given as a function of the normalised speed $V/C_R(\alpha)$ in Fig. 8(a) and as a function of the normalised speed $V/C_R(0)$ in Fig. 8(b) for $\alpha = 0.05, 0.1, 0.2, 1, 3$ (where $V \le C_R(\alpha)$, see (7.5)).

As discussed in the previous section, at low speeds the model presented here does not describe the propagation of the crack through the inhomogeneous lattice accurately. This is due to the highly oscillatory behaviour of the argument of L and it leads to regions of instability, represented by the non-smooth behaviour in G_0/G for low speeds as seen in Fig. 6. Since the expression $K_I/\sqrt{G_0}$ contains the ratio $\sqrt{G/G_0}$ (see (7.1) and (8.4)), we also see a similar behaviour in $K_I/\sqrt{G_0}$ in Fig. 8(a) and (b). For those speeds in this unstable region there is little physical significance of the results presented in the figures below. As we increase the speed of the crack, we leave the region of instability, and the stress intensity factor becomes a smooth function of the crack speed, and tends to a finite value for V tending to the critical surface wave speed $C_R(\alpha)$ in (7.5), as shown in Fig. 8(a). For $\alpha < 1$, in the vicinity of $C_R(\alpha)$, K_I is a monotonically decreasing function for increasing V. When $\alpha \ge 1$, outside the instability region, K_I passes through a global minimum before the converging to a finite value at $C_R(\alpha)$. From the figure, we can see that overall the behaviour of the stress intensity factor is increasing as we decrease the stiffness contrast α.

9. Conclusions

The paper has brought together analytical insight on a propagating semi-infinite fault in an elastic lattice with the computational experiments and physical interpretation of the fields in such a lattice structure. One of the important issues discussed here is the crack stability for different regimes of the crack speed and different values of elastic parameters of the anisotropic lattice.

Although it appears that the analytical solution has a serious limitation due to the assumption of the steady crack propagation, it has been shown in Mishuris et al. (2009a) that in the non-steady regime the averaging procedure appears to be viable. In this case, the averaged solution follows the prediction of the linear model constructed for the case of the steady crack propagation through the lattice.

It is also noted that the model predicts a low-speed unsteady regime, consistent with the results obtained by other approaches (see, for example, Marder and Gross, 1995), for an accelerating crack at the initial stage (low speed) of the crack advance. Although the model formally shows oscillations of the energy release rate ratio in this regime, it is not designed to describe a true physical behaviour of a lattice system with a crack for low values of the crack speed. Hence we do not associate any particular physical effects with these oscillations and simply refer to such a region as the region of instability, where the crack is likely to exhibit a transient behaviour.

Acknowledgements

M.J. Nieves would like to acknowledge the financial support of the U.K. Engineering and Physical Sciences Research Council through the research Grant EP/H018239/1. Support through European Grant FP7-PEOPLE-IAPP (PIAPP-GA-284544-PARM-2), held by G.S. Mishuris, is also gratefully acknowledged.

Appendix A. The sign of L_0

In this section we show that for $V \le C_R$ and $\alpha > 0$ the constant L_0 in (4.19) of Proposition 3, Section 4, is positive.

Note that by Proposition 1, for $V_*^2 \le C_R^2 m/\mu_2$

$$3 - 8V_*^2 > 0, \quad 2V_*^2 - 3\alpha < 0 \tag{A.1}$$

and

$$V_*^4 - \frac{1}{2}(2\alpha+1)V_*^2 + \frac{3\alpha}{8} > 0. \tag{A.2}$$

Also, owing to (4.9)

$$\sqrt{d_1 d_2} = 8\sqrt{3}\sqrt{V_*^4 - \frac{2\alpha+1}{2}V_*^2 + \frac{3}{8}\left(\alpha + \frac{1}{8}\right)} > 0, \tag{A.3}$$

since here the quadratic function of V_*^2, under the square root, was shown in the proof of Proposition 2 to be positive for $V_*^2 \le C_R^2 m/\mu_2$.

Proposition 4. *For $\alpha > 0$, $V_*^2 \le C_R^2 m/\mu_2$ the constant L_0 in (4.19) is positive.*

Proof. *Part 1.* Consider the cases when (a) $\alpha \ge 1$, $0 < V_*^2 \le C_R^2 m/\mu_2$ or (b) $-1/2+\sqrt{2} \le \alpha \le 1$ so that $\frac{3}{2}[\alpha-1+\sqrt{1-\alpha}] \le V_*^2 \le C_R^2 m/\mu_2$.

For the parameter values in both (a) and (b), M_0 defined in (4.10) is nonnegative.

We show that B_1 in (4.20) is negative, which implies B_2 is also negative. The inequality $B_1 < 0$ gives

$$2V_*^4 - 3(\alpha+1)V_*^2 + \frac{9}{4}\alpha > V_*^2 M_0. \tag{A.4}$$

Here, this is valid for

$$V_*^2 < \frac{3(\alpha+1-\sqrt{\alpha^2+1})}{4},$$

which is the case, since

$$\frac{C_R^2 m}{\mu_2} = \frac{2\alpha+1-\sqrt{3\alpha^2+(\alpha-1)^2}}{4} < \frac{3(\alpha+1-\sqrt{\alpha^2+1})}{4} \quad \text{for } \alpha > 0.$$

Indeed, the above provides us with

$$3\sqrt{\alpha^2+1} - \sqrt{3\alpha^2+(\alpha-1)^2} < \alpha+2, \tag{A.5}$$

and the left-hand side is positive as a result of

$$9(\alpha^2+1) > 3\alpha^2+(\alpha-1)^2.$$

Thus from (A.5) we have

$$(\alpha^2+1)(3\alpha^2+(\alpha-1)^2) - (2\alpha^2-\alpha+1)^2 = 2\alpha^3 > 0 \quad \text{for } \alpha > 0.$$

Then (A.4) leads to

$$\frac{3}{16}(8V_*^2-3)(4V_*^2-3\alpha)^2 < 0,$$

if $V_*^2 < 3/8$, and this holds by Proposition 1. Therefore $B_j < 0$, for $j=1, 2$. This together with (A.1)–(A.3) shows $L_0 > 0$. □

Part 2. Consider the cases when (c) $0 < \alpha < -1/2+\sqrt{2}$, $0 < V_*^2 \le C_R^2 m/\mu_2$ or (d) $-1/2+\sqrt{2} \le \alpha \le 1$, $0 < V_*^2 \le \frac{3}{2}[\alpha-1+\sqrt{1-\alpha}]$.

For the parameter values in cases (c) and (d), M_0 in (4.10) is purely imaginary and can be written as

$$M_0 = \mathrm{i}R_0, \quad R_0 = \sqrt{3(1-\alpha)(3\alpha-4V_*^2)-4V_*^4}, \tag{A.6}$$

where according to the proof of Proposition 2, $R_0^2 > 0$ since $V_*^2 \le C_R^2 m/\mu_2$. Then

$$d_2 = \overline{d_1} \quad \text{and} \quad B_2 = \overline{B_1},$$

and from (4.19)

$$L_0 = \frac{\sqrt{3}\,|d_1|\,\mathrm{Re}(\overline{B_1}\sqrt{d_1})}{(3-8V_*^2)(2V_*^2-3\alpha)(V_*^4-\frac{1}{2}(2\alpha+1)V_*^2+\frac{3\alpha}{8})}.$$

By (A.1)–(A.3) it remains to show that $\mathrm{Re}(\overline{B_1}\sqrt{d_1})$ is negative. We have

$$\mathrm{Re}(\overline{B_1}\sqrt{d_1}) = \mathrm{Re}(B_1)\,\mathrm{Re}(\sqrt{d_1}) + \mathrm{Im}(B_1)\,\mathrm{Im}(\sqrt{d_1}),$$

with

$$\mathrm{Re}(B_1) = -\frac{1}{3}V_*^4 + \frac{\alpha+1}{2}V_*^2 - \frac{3}{8}\alpha, \quad \mathrm{Im}(B_1) = \frac{1}{6}V_*^2 R_0 > 0. \tag{A.7}$$

Note that due to (A.6) and (4.9), $-\pi/2 < \arg(\sqrt{d_1}) < 0$, therefore

$$\mathrm{Re}(\sqrt{d_1}) > 0, \quad \mathrm{Im}(\sqrt{d_1}) < 0. \tag{A.8}$$

The roots of $\mathrm{Re}(B_1)$, which is treated as a quadratic function of V_*^2, are

$$v_\pm^2 = \frac{3}{4}[\alpha+1 \pm \sqrt{\alpha^2+1}] > 0 \quad \text{for } \alpha > 0.$$

Considering case (d), we have

$$V_*^2 < \nu_-^2 \quad \text{for } 3/4 < \alpha \le 1,$$

and then $\mathrm{Re}(B_1) < 0$. This with (A.7), (A.8) implies $\mathrm{Re}(\overline{B_1}\sqrt{d_1})$ is negative and part (d) is proved.

Returning to part (c), for $\mathrm{Re}(B_1) < 0$ we require

$$\frac{2\alpha+1-\sqrt{3\alpha^2+(\alpha-1)^2}}{4} < \nu_-^2,$$

which was shown to be valid for $\alpha > 0$ in the proof of Proposition 2, Section 4. Therefore, the proof is complete. □

Appendix B. Poles of L

Here, for $\mu_1 = \mu_2 = 1$, we verify the inequalities (5.10) and (5.11) hold, which indicate when the functions (5.8) and (5.9) are solutions of (5.1), respectively.

For $\xi \in [0,4\pi]$, $\mathrm{sign}\{r(\Lambda_1^*)/r(\Lambda_2^*)\} = 1$ when $V = \pm\Omega_2^{(D)}/\xi$. By direct substitution of (5.8) into (5.1) we obtain

$$q\big|_{V=\pm\Omega_2^{(D)}/\xi} = \frac{3}{2}\mathrm{i}r(\Lambda_1^*)\sin^2(\xi/2)|\tan(\xi/2)|\,|4\cos^2(\xi/2)-1|\,\{T_1(\xi)-T_2(\xi)\}, \tag{B.1}$$

where

$$T_j(\xi) = \mathrm{sign}\{2(1+(-1)^j\,\mathrm{sign}\{\cos(\xi/2)\})\cos^2(\xi/2)-1\}, \quad j = 1,2.$$

The factor in front of the curly braces in (B.1), is zero when $\xi = 0, \frac{2}{3}\pi, \frac{4}{3}\pi, 2\pi, \frac{8}{3}\pi, \frac{10}{3}\pi, 4\pi$, and is singular at $\xi = \pi$ and 3π.

We now show that (B.1) is zero in the neighbourhood of these poles, by solving the equation

$$T_1(\xi) - T_2(\xi) = 0.$$

For $\xi = \pi, 3\pi$ it is clear this equation is satisfied. When $\xi \neq \pi, 3\pi$, we are left to determine when the inequality

$$1 - 4\cos^2(\xi/2) > 0$$

is satisfied. This occurs for $\xi \in [\frac{2}{3}\pi, \frac{4}{3}\pi] \cup [\frac{8}{3}\pi, \frac{10}{3}\pi]$. The above is confirmed in Fig. 9.

Next, insertion of (5.9) into (5.1) yields

$$q\big|_{V=\pm\Omega_3^{(D)}/\xi} = \frac{\mathrm{i}\sqrt{3}\sin^2(\xi/2)|\sin(\xi/2)|(2\cos(\xi/2)-1+\sqrt{3})\sqrt{\sqrt{3}-2\sin^2(\xi/2)}}{2\sqrt{2\cos^2(\xi/2)+\sqrt{3}}}\{r(\Lambda_1^*)+r(\Lambda_2^*)\}. \tag{B.2}$$

The factor outside the curly braces in (B.2), for $\xi \in [0,4\pi]$, has the roots $\xi = 0, 0.7614\pi, 1.2386\pi, 2\pi, 2.7614\pi, 3.283\pi$ and 4π. We must have $\mathrm{sign}\{r(\Lambda_1^*)/r(\Lambda_2^*)\} = -1$ when $V = \pm\Omega_3^{(D)}/\xi$. Fig. 10, shows the plot of $\mathrm{sign}\{r(\Lambda_1^*)/r(\Lambda_2^*)\}$ in this case, and we see that this condition holds provided ξ satisfies the inequalities of (5.11).

Appendix C. Asymptotic properties of L

We now state and prove some properties of the kernel function L, which are used in the analysis of the Wiener–Hopf equation (4.5), in Section 6.

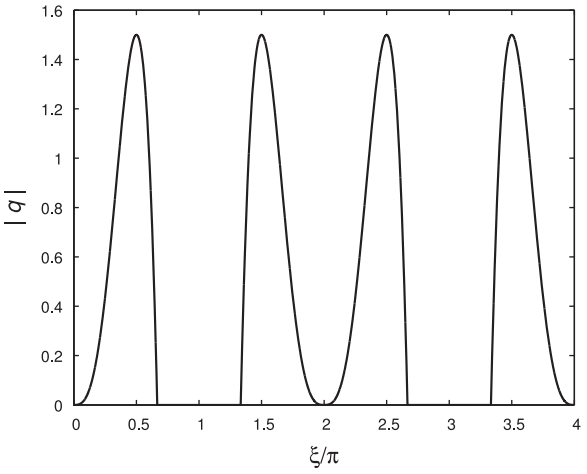

Fig. 9. The plot of the absolute value of q in (B.1) as a function of the normalised wave number, when $V = \pm\Omega_2^{(D)}/\xi$.

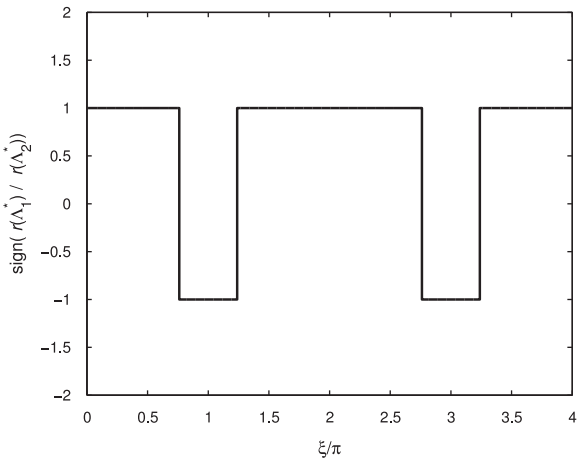

Fig. 10. The sign of the ratio of $r(\Lambda_1^*)$ to $r(\Lambda_2^*)$ as a function of ξ/π, when $V=\pm\Omega_3^{(D)}/\xi$.

Lemma 1. *$L(\varepsilon+i\xi V,\xi)\to 1$ as $|\xi|\to\infty$.*

Proof. According to (4.11), for $|\xi|\to\infty$, we have

$$\Lambda_j^*=\frac{1}{2z_j}+O(|z_j|^{-3}),\quad \text{and}\quad r(\Lambda_j^*)=1,\ j=1,2,$$

$$\sqrt{z_j^2-1}=z_j+O(|\xi|^{-2}), \tag{C.1}$$

$$F(z_j)=3z_j^2-\frac{m}{\mu_2}(\varepsilon+i\xi V)^2 z_j[2\cos(\xi/2)+1]+O(|\xi|^2).$$

Since $z_j=O(|\xi|^2)$ for $|\xi|\to\infty$, then

$$F(z_2)\sqrt{z_1^2-1}-F(z_1)\sqrt{z_2^2-1}=3z_1z_2(z_2-z_1)+O(|\xi|^4),$$

$$3(z_2-z_1)\sqrt{z_1^2-1}\sqrt{z_2^2-1}=3z_1z_2(z_2-z_1)+O(|\xi|^2).$$

The leading order term in both of the above estimates is $O(|\xi|^6)$ for $|\xi|\to\infty$, therefore

$$L(\varepsilon+i\xi V,\xi)=1+O(|\xi|^{-2}),\quad |\xi|\to\infty. \qquad \square$$

Next we state

Lemma 2. *For the product of two complex functions $f(\xi)$, $g(\xi)\in\mathcal{J}$, we have $(fg)(\xi)\in\mathcal{J}$.*

This leads to

Lemma 3. *For $\xi\in\mathbb{R}$, $\varepsilon>0$, we have $L(\varepsilon+i\xi V,\xi)\in\mathcal{J}$.*

Proof. The term

$$\frac{m}{\mu_2}(\varepsilon^2-\xi^2V^2+2i\xi\varepsilon V)\in\mathcal{J},$$

since it has an even real part and odd imaginary part with respect to ξ. This together with Lemma 2 and (3.5) shows that $z_j\in\mathcal{J}$, $j=1,2$. and hence, after a second application of Lemma 2 with (4.6) we complete the proof.

Now we consider the index of the function $L(\varepsilon+i\xi V,\xi)$ which defined by

$$\mathrm{Ind}(L(\varepsilon+i\xi V,\xi))=\lim_{\xi\to\infty}\frac{1}{2\pi}[\arg(L(\varepsilon+i\xi V,\xi))-\arg(L(\varepsilon-i\xi V,-\xi))]. \tag{C.2}$$

This quantity can also be interpreted as the number of times the path traced by L in the complex plane for $\xi \in (-\infty,\infty)$ winds around the origin. We have

Lemma 4. *For* $\varepsilon > 0$, *we have* $\mathrm{Ind}(L(\varepsilon+\mathrm{i}\xi V,\xi)) = 0$.

Proof. According to Section 6, if $\xi = \xi^*$ represents a root or a pole of L such that $V < V_g$ ($V > V_g$), then the regularisation parameter ε shifts this root or pole into lower (upper) half of the complex plane. Correspondingly, $\xi = -\xi^*$ is then a root or a pole of L such that $V > V_g$ ($V < V_g$) and this will be located in the upper (lower) half of the complex plane after the regularisation of L. Therefore, $L(\varepsilon+\mathrm{i}\xi V,\xi)$ has an equal number of roots in the upper and lower half planes and an equal number of poles in the upper and lower half planes, and these numbers are independent of ε. Hence it is sufficient to show that for large ε, $\mathrm{Ind}(L(\varepsilon+\mathrm{i}\xi V,\xi)) = 0$.

First assume ξ, $\varepsilon \gg 1$, so that $|\varepsilon+\mathrm{i}\xi V| \gg 1$, then

$$z_j = O(\varepsilon^2+\xi^2V^2), \quad \Lambda_j^* = \frac{1}{2z_j} + O\left(\frac{1}{(\varepsilon^2+\xi^2V^2)^3}\right),$$

and so

$$r(\Lambda_j^*) = 1, \quad 3(z_2-z_1)\sqrt{z_1^2-1}\sqrt{z_2^2-1} = 3z_1z_2(z_2-z_1)+O(\varepsilon^2+\xi^2V^2),$$

and

$$F(z_2)\sqrt{z_1^2-1}-F(z_1)\sqrt{z_2^2-1} = 3z_1z_2(z_2-z_1)-\frac{m}{\mu_2}(\varepsilon+\mathrm{i}\xi V)^2(z_2-z_1)(2+\cos(\xi/2))+O(\varepsilon^2+\xi^2V^2).$$

Thus, from (4.6),

$$L(\varepsilon+\mathrm{i}\xi V,\xi) = 1+\frac{m(\varepsilon+\mathrm{i}\xi V)^2[2+\cos(\xi/2)]}{3\mu_2 z_1 z_2} + O\left(\frac{1}{(\varepsilon^2+\xi^2V^2)^2}\right), \quad \varepsilon^2+\xi^2V^2 \to \infty, \tag{C.3}$$

where according to (3.5), z_1z_2 is $O((\varepsilon^2+\xi^2V^2)^2)$. The remainder estimate here is uniform for large ε and ξ.

The plot of the contour traced by $L(\varepsilon+\mathrm{i}\xi V,\xi)$ for large ε and ξ, with $m = \mu_1 = \mu_2 = 1$ ($\alpha = 1$), $V = 0.3941$, can be found in Fig. 11. In this figure both the plot given by (4.6) and the leading order term of (C.3) are presented, and it can be seen there is a good agreement between both computations. When $\varepsilon \gg \xi$, from (C.3)

$$L(\varepsilon+\mathrm{i}\xi V,\xi) = 1+\frac{\mu_2(2+\cos(\xi/2))}{m}\left[\frac{1}{\varepsilon^2}-\frac{2\mathrm{i}\xi V}{\varepsilon^3}\right]+O\left(\frac{1}{\varepsilon^4}\right), \quad \varepsilon \to \infty,$$

and this asymptotic expression (C.3) implies that for large ε the contour traced by L does not cross the negative real axis, since to leading order the above real part is always positive, whereas the imaginary part can cross the real axis for $\xi \in (-\infty,\infty)$. Similar behaviour can be seen in Fig. 11, where the contour traced by $L(\varepsilon+\mathrm{i}\xi V,\xi)$ for $\xi \in (-400\pi,400\pi)$ in the complex plane forms a closed loop which passes through 1. Therefore, $\mathrm{Ind}(L(\varepsilon+\mathrm{i}\xi V,\xi)) = 0$ in the limit $\varepsilon \to \infty$ and this also holds for all $\varepsilon > 0$. □

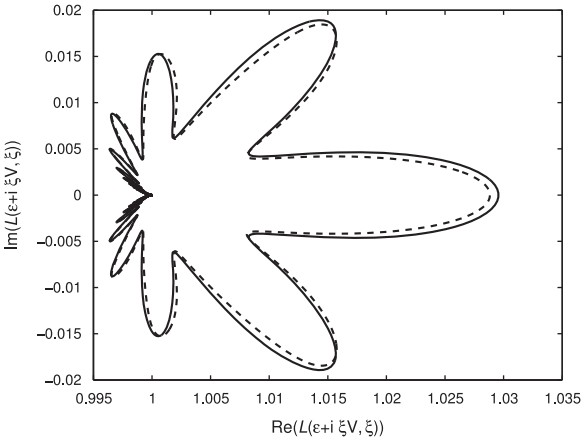

Fig. 11. The contour traced by $L(\varepsilon+\mathrm{i}\xi V,\xi)$ in the complex plane for $\varepsilon = 10$, $m = \mu_1 = \mu_2 = 1$, ($\alpha = 1$), $V = 0.3941$, $\xi/\pi \in [-400,400]$. The computations for the solid curve are based on formula (4.6) and those for the dashed curve are based on the leading order part of (C.3).

The next two corollaries provide us with additional properties of L needed for the factorisation of (4.5). As a corollary of Lemma 3 we have

Corollary 1. *For* $\xi \in \mathbb{R}$, $\varepsilon > 0$,

$$\arg(L(\varepsilon+\mathrm{i}\xi V,\xi)) = -\arg(L(\varepsilon-\mathrm{i}\xi V,-\xi)).$$

Owing to (C.2), Lemma 4 and Corollary 1 we also have

Corollary 2. *For* $\varepsilon > 0$, $\arg(L(\varepsilon+\mathrm{i}\xi V,\xi)) = 0$ *as* $\xi \to \pm\infty$.

Appendix D. Solution of the Wiener–Hopf equation (6.3) for a particular load

In order to determine the functions $\mathcal{S}_+$ and $\mathcal{S}_-$, as solutions of the Wiener–Hopf equation (6.3), for the sake of simplicity, we consider a certain type of "load" ϕ^F which produces simple examples for the additive split $P_+ + P_-$ in the right-hand side of (6.3).

Let $\mathcal{P}_+$ ($\mathcal{P}_-$) be the set of poles and $\mathcal{Z}_+$ ($\mathcal{Z}_-$) the set of zeros of $L(\varepsilon+\mathrm{i}\xi V,\xi)$ that are located in the upper (lower) half plane. The first factor in the right-hand side of (6.3) is singular at the zeros of L_- and the singular points of L_+. Assume $\xi_p^- \in \mathcal{P}_-$, and

$$L_+(\varepsilon+\mathrm{i}\xi V,\xi) \sim \frac{A_p}{[\zeta_-\varepsilon-\mathrm{i}(\xi-\xi_p^-)]^a}, \quad a>0, \varepsilon \to +0, \tag{D.1}$$

where $\zeta_- = 1/(V_g - V)$ for $\xi \to \xi_p^-$. Also, suppose for $\xi_z^+ \in \mathcal{Z}_+$

$$L_-(\varepsilon+\mathrm{i}\xi V,\xi) \sim A_z[\zeta_+\varepsilon+\mathrm{i}(\xi-\xi_z^+)]^b, \quad b>0, \varepsilon \to +0, \tag{D.2}$$

for $\xi \to \xi_z^+$ and $\zeta_+ = 1/(V - V_g)$. Here, ξ_p^- is a pole and ξ_z^+ is a zero of L located in the lower and upper half of the complex plane, respectively, and the constants A_p and A_z depend on α.

We consider two examples of the function ϕ

(a)

$$\phi_A(\eta) = \phi(\eta) = -C_A(2\zeta_-\varepsilon)^a \exp[(\zeta_-\varepsilon-\mathrm{i}\xi_p^-)\eta]H(-\eta), \tag{D.3}$$

and after taking the Fourier transform, we have

$$\phi_{A,-} = -\frac{(2\zeta_-\varepsilon)^a C_A}{[\zeta_-\varepsilon+\mathrm{i}(\xi-\xi_p^-)]}, \quad \phi_{A,+} = 0, \tag{D.4}$$

and (b)

$$\phi_B(\eta) = \phi(\eta) = C_B(2\zeta_+\varepsilon)^b \exp[-(\zeta_+\varepsilon+\mathrm{i}\xi_z^+)\eta]H(\eta).$$

so that

$$\phi_{B,+} = \frac{(2\zeta_+\varepsilon)^b C_B}{[\zeta_+\varepsilon-\mathrm{i}(\xi-\xi_z^+)]}, \quad \phi_{B,-} = 0. \tag{D.5}$$

In cases (a) and (b), we have C_A and C_B are constants representing the intensity of the load. Also

$$\lim_{\varepsilon\to+0}\phi_A(\eta) = \lim_{\varepsilon\to+0}\phi_B(\eta) = 0. \tag{D.6}$$

Right-hand side of (6.3) *for the load of case* (*a*). We insert (D.4) into (6.3) and taking the limit as $\varepsilon \to +0$ and noting that due to (D.6)

$$\lim_{\varepsilon\to+0}\frac{\phi_{A,-}}{L_-} = 0,$$

we have using (D.1)

$$L_+\mathcal{S}_+ + \frac{\mathcal{S}_-}{L_-} = \frac{A_p C_A}{\mu_2}\lim_{\varepsilon\to+0}\frac{(2\zeta_-\varepsilon)^a}{[\zeta_-\varepsilon-\mathrm{i}(\xi-\xi_p^-)]^a[\zeta_-\varepsilon+\mathrm{i}(\xi-\xi_p^-)]}.$$

Here, according to Slepyan (2002, Section 2.2.4), the above limit results in the appearance of the Dirac delta function, therefore

$$L_+\mathcal{S}_+ + \frac{\mathcal{S}_-}{L_-} \sim \frac{2\pi A_p C_A}{\mu_2}\delta(\xi-\xi_p^-) = \frac{A_p C_A}{\mu_2}\left[\frac{1}{\varepsilon+\mathrm{i}(\xi-\xi_p^-)} + \frac{1}{\varepsilon-\mathrm{i}(\xi-\xi_p^-)}\right], \quad \varepsilon \to +0.$$

Right-hand side of (6.3) for the load of case (b). Similarly, using (D.2), (D.5) and

$$\lim_{\varepsilon\to+0}\phi_{B,+}L_+=0,$$

by Slepyan (2002, Section 2.2.4), we have

$$L_+\mathcal{S}_+ + \frac{\mathcal{S}_-}{L_-} = \lim_{\varepsilon\to+0}\frac{\mathcal{C}_B}{\mu_2 A_z}\frac{(2\zeta_+\varepsilon)^b}{[\zeta_+\varepsilon+\mathrm{i}(\xi-\xi_z^+)]^b[\zeta_+\varepsilon-\mathrm{i}(\xi-\xi_z^+)]}$$
$$\sim 2\pi\frac{\mathcal{C}_B}{\mu_2 A_z}\delta(\xi-\xi_z^+)=\frac{\mathcal{C}_B}{\mu_2 A_z}\left[\frac{1}{\varepsilon+\mathrm{i}(\xi-\xi_z^+)}+\frac{1}{\varepsilon-\mathrm{i}(\xi-\xi_z^+)}\right],\quad \varepsilon\to 0.$$

General solution of (6.3). Consulting the above cases (a) and (b), by linear superposition the right-hand side of (6.3) has the form

$$L_+\mathcal{S}_+ + \frac{\mathcal{S}_-}{L_-} = \frac{1}{\mu_2}\sum_{\xi_p\in\mathcal{P}_-}\mathcal{A}_p\left[\frac{1}{\varepsilon+\mathrm{i}(\xi-\xi_p)}+\frac{1}{\varepsilon-\mathrm{i}(\xi-\xi_p)}\right]+\frac{1}{\mu_2}\sum_{\xi_z\in\mathcal{Z}_+}\mathcal{B}_z\left[\frac{1}{\varepsilon+\mathrm{i}(\xi-\xi_z)}+\frac{1}{\varepsilon-\mathrm{i}(\xi-\xi_z)}\right],$$

for $\varepsilon\to 0$, where $\mathcal{A}_p$ and $\mathcal{B}_p$ are arbitrary complex constants.

Then the functions $\mathcal{S}_+$ and $\mathcal{S}_-$ are given by

$$\mathcal{S}_+ = \frac{1}{\mu_2 L_+(\xi)}\left[\sum_{\xi_p\in\mathcal{P}_-}\frac{\mathcal{A}_p}{\varepsilon-\mathrm{i}(\xi-\xi_p)}+\sum_{\xi_z\in\mathcal{Z}_+}\frac{\mathcal{B}_z}{\varepsilon-\mathrm{i}(\xi-\xi_z)}\right],$$
$$\mathcal{S}_- = \frac{L_-(\xi)}{\mu_2}\left[\sum_{\xi_p\in\mathcal{P}_-}\frac{\mathcal{A}_p}{\varepsilon+\mathrm{i}(\xi-\xi_p)}+\sum_{\xi_z\in\mathcal{Z}_+}\frac{\mathcal{B}_z}{\varepsilon+\mathrm{i}(\xi-\xi_z)}\right],\tag{D.7}$$

where $\varepsilon\to+0$. In Section 6, (6.4) follows by considering terms in (D.7) which correspond to $\xi_p^-=0$ in (D.1) and (D.3).

Appendix E. Evaluation of $L_\pm$ for $\xi\to 0$

Now, using the Cauchy-type integral of (6.2) and the asymptotic representation (4.18) for L when $\xi\to 0$, we derive asymptotes of the functions $L_\pm$ near zero, found in (7.2). The logarithmic term in (6.2) is rewritten as

$$\ln L(\varepsilon+\mathrm{i}\xi V,\xi)=\ln|L(\varepsilon+\mathrm{i}\xi V,\xi)|+\mathrm{i}\arg(L(\varepsilon+\mathrm{i}\xi V,\xi)).$$

Then

$$L_\pm(\varepsilon+\mathrm{i}\xi V,\xi)=\exp\left(\pm\frac{1}{2\pi\mathrm{i}}\int_{-\infty}^{\infty}\frac{\ln|L(\varepsilon+\mathrm{i}sV,s)|}{s-\xi}\,ds\right)$$
$$\times\exp\left(\pm\frac{1}{2\pi}\int_{-\infty}^{\infty}\frac{\arg(L(\varepsilon+\mathrm{i}sV,s))}{s-\xi}\,ds\right).\tag{E.1}$$

The first exponent on the right, by the Cauchy theorem, defines the modulus of $L(\varepsilon+\mathrm{i}\xi V,\xi)$, whereas the second exponent, owing to the expansion

$$\frac{1}{s-\xi}=\sum_{n=0}^{\infty}\frac{\xi^n}{s^{n+1}}$$

yields

$$\exp\left(\pm\frac{1}{2\pi}\int_{-\infty}^{\infty}\frac{\arg(L(\varepsilon+\mathrm{i}sV,s))}{s-\xi}\,ds\right)\sim\exp\left(\pm\frac{1}{2\pi}\int_{-\infty}^{\infty}\frac{\arg(L(\varepsilon+\mathrm{i}sV,s))}{s}\,ds\right),$$

for $\xi\to 0$. The integrand in the right-hand side is an even function as a result of Corollary 1, and so

$$\exp\left(\pm\frac{1}{2\pi}\int_{-\infty}^{\infty}\frac{\arg(L(\varepsilon+\mathrm{i}sV,s))}{s-\xi}\,ds\right)\sim\exp\left(\pm\frac{1}{\pi}\int_{0}^{\infty}\frac{\arg(L(\varepsilon+\mathrm{i}sV,s))}{s}\,ds\right).$$

Therefore, allowing $\xi\to+0$ in (E.1), and using Proposition 3, we obtain (7.2).

References

Colquitt, D.J., Nieves, M.J., Jones, I.S., Movchan, N.V., Movchan, A.B., 2012. Trapping of a crack advancing through an elastic lattice. Int. J. Eng. Sci. 61, 129–141.
Fineberg, J., Marder, M., 1999. Instability in dynamic fracture. Phys. Rep. 313, 1–108.
Marder, M., Gross, S., 1995. Origin of crack tip instabilities. J. Mech. Phys. Solids 43 (1), 1–48.
Marder, M., Liu, Xiangming, 1993. Instability in lattice fracture. Phys. Rev. Lett. 71 (15), 2417–2420.

Mishuris, G.S., Movchan, A.B., Slepyan, L.I., 2007. Waves and fracture in an inhomogeneous lattice structure. Waves Random Complex Media 17, 409–428.
Mishuris, G.S., Movchan, A.B., Slepyan, L.I., 2008. Dynamical extraction of a single chain from a discrete lattice. J. Mech. Phys. Solids 56, 487–495.
Mishuris, G.S., Movchan, A.B., Slepyan, L.I., 2009a. Localised knife waves in a structured interface. J. Mech. Phys. Solids 57, 1958–1979.
Mishuris, G.S., Movchan, A.B., Slepyan, L.I., 2009b. Localization and dynamic defects in lattice structures. Ruiz, P.D., Silberschmidt, V.V. (Eds.), Computational and Experimental Mechanics of Advanced Materials, CISM International Centre for Mechanical Sciences, vol. 514, Springer, pp. 51–82.
Slepyan, L.I., 2001a. Feeding and dissipative waves in fracture and phase transition. I. Some 1D structures and a square-cell lattice. J. Mech. Phys. Solids 49, 469–511.
Slepyan, L.I., 2001b. Feeding and dissipative waves in fracture and phase transition. III. Triangular-cell lattice. J. Mech. Phys. Solids 49, 2839–2875.
Slepyan, L.I., 2002. Models and Phenomena in Fracture Mechanics. Springer, Berlin.
Slepyan, L.I., Ayzenberg-Stepanenko, M.V., 2002. Some surprising phenomena in weak-bond fracture of a triangular lattice. J. Mech. Phys. Solids 50, 1591–1625.
Slepyan, L.I., Movchan, A.B., Mishuris, G.S., 2010. Crack in a lattice waveguide. Int. J. Fract. 162, 91–106.